Activated Carbon Derived from *Biomass* Combustion Bottom Ash as Solid Sorbent for CO_2 Adsorption

Mikhail Gorbounov, Ben Petrovic, Serap Ozmen, Peter Clough, Salman Masoudi Soltani

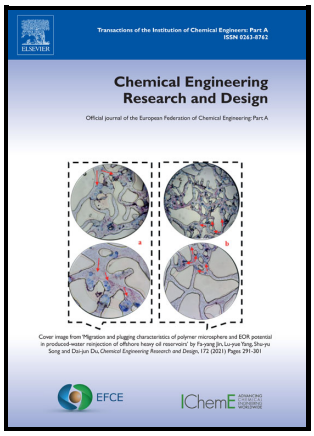

PII: S0263-8762(23)00269-1

DOI: https://doi.org/10.1016/j.cherd.2023.04.057

Reference: CHERD5597

To appear in: *Chemical Engineering Research and Design*

Received date: 18 January 2023
Revised date: 3 April 2023
Accepted date: 25 April 2023

Please cite this article as: Mikhail Gorbounov, Ben Petrovic, Serap Ozmen, Peter Clough and Salman Masoudi Soltani, Activated Carbon Derived from *Biomass* Combustion Bottom Ash as Solid Sorbent for CO_2 Adsorption, *Chemical Engineering Research and Design,* (2023) doi:https://doi.org/10.1016/j.cherd.2023.04.057

Activated Carbon Derived from *Biomass* Combustion Bottom Ash as Solid Sorbent for CO_2 Adsorption

Mikhail Gorbounov[a], Ben Petrovic[a], Serap Ozmen[b], Peter Clough[b], Salman Masoudi Soltani[a,*]

[a]Department of Chemical Engineering, Brunel University London, Uxbridge UB8 3PH, UK

[b]Energy and Power Theme, Cranfield University, Cranfield, Bedfordshire MK43 0AL, UK

Corresponding author's telephone: +44-(0)1895265884
Corresponding author's email: Salman.MasoudiSoltani@brunel.ac.uk

Abstract

Climate change and global warming, caused mainly by the anthropogenic CO_2 emissions, has been recognised to be the biggest threat to global ecosystems. Replacing fossil fuels with *sustainable* biomass for heat and power generation is a key tool in our fight against climate change. Such combustion, however, generates large quantities of ash which, unlike the coal counterparts, are yet to find major applications in industry. This leads to challenging waste management and thus, necessitating urgent measures to valorise this increasing waste stream. However, producing activated carbon from biomass combustion ash allows for not only effective waste valorisation into value-added products, but also to prepare a sorbent for post-combustion carbon capture from an abundant and cheap source that is readily available for *in-situ* application (hence, minimising overall costs). This work has focused on preparation and activation of industrial-grade *biomass* ash-derived porous carbon *via* an economical direct method, followed by an extensive characterisation of its textural properties as well as an evaluation of the CO_2 uptake of both the virgin and the activated carbonaceous sorbents. The final sample was selected based on an extensive optimisation campaign aiming towards maximisation of yield and CO_2 uptake. The optimum activated sample adsorbed 0.69 mmol/g, thus, nearly doubling the adsorption capacity of the virgin biomass combustion bottom ash-derived carbon.

Graphical abstract

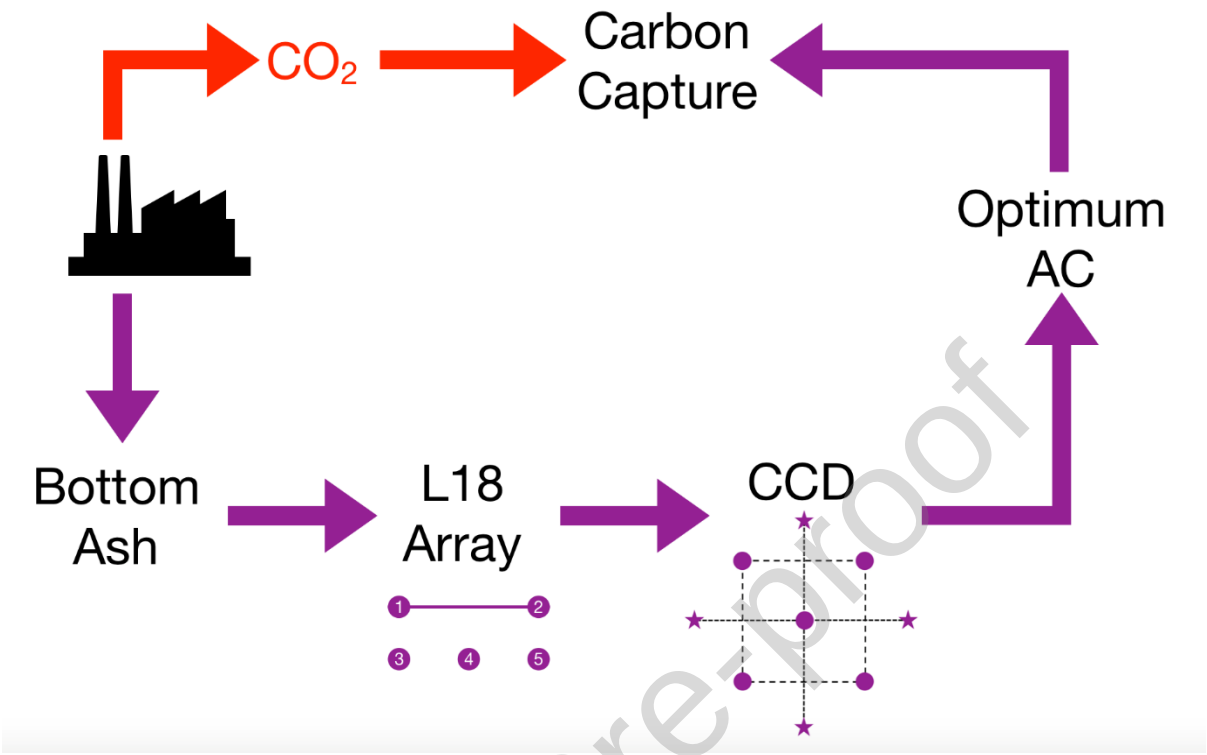

Key words: Post-combustion Carbon Capture, Adsorption, Biomass Combustion Ash, Bottom Ash, Activated Carbon

1. Introduction

Climate change and global warming is a major global challenge today. This is mainly caused by an overwhelming amount of anthropogenic CO_2 emissions, a lion's share of which stemming from the energy and power sector. In the UK, for instance, nearly 100 Mt of CO_2eq (~ 20% of the total) emissions arise from the electricity and heat production alone.

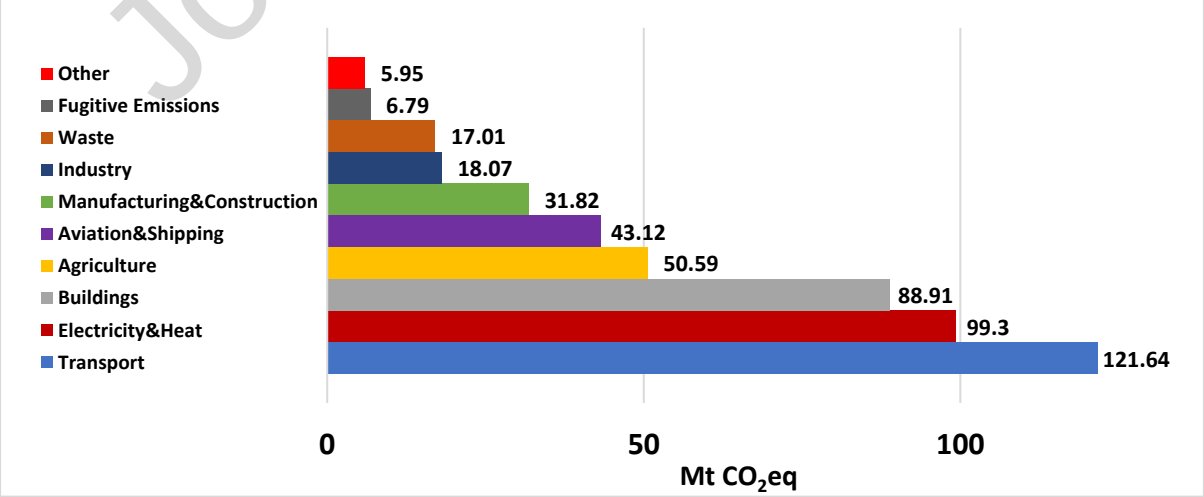

Figure 1. Greenhouse gas emissions by sector, UK, 2019. Reproduced from (Ritchie, Roser and Rosado, 2020).

Many processes have been conceptualised and/or developed to battle global warming. Among these, transition to green energy and other net-zero emission technologies have been attracting significant attention within the past few years. Carbon Capture and Storage (CCS) has often been considered a pivotal technology to limit the temperature rise to 2 °C by immobilising the anthropogenic CO_2 emissions (Sevilla and Fuertes, 2011; García-Díez *et al.*, 2021; Petrovic *et al.*, 2021). Based on the data from 2022, there are 29 operational facilities worldwide predominantly located in North America, namely, 12 in the USA, and 4 in Canada (Orenstein and Cooke, 2022), though, none in the UK as of early 2023. As such, the UK Government has recently announced plans to invest £20 billion in CCS over the coming two decades (Dixon, 2023). Nevertheless, the prolonged combustion of fossil fuels has led to a considerable increase in the atmospheric carbon dioxide concentration that most probably cannot be mitigated without timely implementation of negative emission technologies (NET) as envisaged by the Intergovernmental Panel on Climate Change (IPCC) (IPCC, 2014). One such approach is the combination of two separate net-zero emission technologies: *bioenergy* and *CCS*. The former technology employs *sustainable* biomass as the primary fuel for heat & power generation, thus not emitting any "new" CO_2 into the atmosphere as the evolved greenhouse gas has been previously adsorbed by the plant during its growth. This approach has been recognised to be essential for reaching the climate change targets, with 85% of the scenarios within the IPCC reports employing bioenergy with carbon capture and storage (BECCS) technologies (IPCC, 2014). Further, the IPCC also underscores the fact that the deployment of biomass for electricity generation would be sustainable in the long term only if coupled with CCS (EASAC, 2018).

One of the major barriers in the widespread implementation of BECCS (and CCS in general) is the cost associated with the process. As a result, in order to propel its deployment, a significant reduction in the price of CO_2 capture is imperative, with the U.S. Department of Energy announcing a target of $30 per metric tonne of CO_2 by 2030 as their goal (Winberg, 2020). Current industrial technologies (i.e. absorption *via* amine solutions) are, however, costly, with the levelized cost of capture for Boundary Dam being ~$115/tonne of CO_2 captured (Global CCS Institute, 2019). A more recent front-end engineering design (FEED) study (Elliott, 2022) suggested the capture cost with monoethanolamine (MEA) to be $114.5/t CO_2. Granted, these numbers are dominated by the capital recovery, however, the energy requirement is also quite costly. For instance, the solvent management at the Petra Nova project in Texas is estimated to cost in the vicinity of $10/t CO_2 alone (Gibbins, 2022). Apart from the highlighted expenditures, their corrosiveness alongside potential formation of hazardous degradation products (e.g. nitrosamines are strong carcinogens) are further incentives for a transition away from the current industrial CCS benchmark of amines for the thermal power sector. A proposed alternative that alleviates the secondary pollution associated with these solvents (e.g. fugitive emissions) as well as corrosion issues is implementing adsorption-based technologies. By using a non-toxic, non-hazardous and non-corrosive sorbent, a significant portion of the highlighted issues can be overcome. Nevertheless, every adsorbent should be "married" to a process that maximises its potential (Sircar, 2002) based on the nature of the governing adsorbate-adsorbent interactions, i.e. a suitable combination of the adsorbent and a particular regeneration mode (electric/pressure(and/or vacuum)/temperature swing (Dhoke *et al.*, 2021) (Raganati, Miccio and Ammendola, 2021) or some combination thereof), an appropriate gas-solid contactor

configuration (fixed (Ammendola *et al.*, 2020)/fluidised (Dietrich *et al.*, 2018)/moving bed and etc.) has to be systematically identified.

Nevertheless, the current trajectories suggest potential for a) *switching from fossil fuels to biomass combustion,* and b) *transitioning away from amine absorption to adsorption with solid sorbents as the capturing technique*. These steps are aimed at not only reducing the greenhouse gas footprint of the thermal power plant but also decreasing secondary environmental impact. Nevertheless, advanced sorbents are often very expensive. For instance, the price of USTA-16, a novel metal-organic framework (MOF) has been shown to cost up to 83,200 €/t of adsorbent (Subraveti *et al.*, 2021). Other MOFs (MIL-53(Al), HKUST-1 and etc.) that are readily available to procure from the biggest chemical producers and/or suppliers also cost in the region of thousands of £ per kg. As such, these substances would not alleviate the economic burden associated with CO_2 capture.

One way of reducing the overall costs is to minimise the material price of the capturing media by using a sorbent that is a*) readily available on site of biomass combustion thermal power plants*, and b) *coming from a waste-source (e.g. combustion bottom ash)*. The latter point is of utter importance as it not only decreases the price for landfilling of the ash whilst simultaneously producing a value-added product, but also provides the additional benefit of waste valorisation. This is also in line with the 2021 UK Biomass Policy Statement ('UK Biomass Policy Statement', 2021), which aims to minimise waste itself alongside the environmental effects of waste management whilst simultaneously maximising its value. With the anticipated increase in bioenergy within the years to come, this would become even more important, both monetarily and societally.

Drax power plant, with a capacity of 3.9 GW_{th}, is one of the largest biomass combustion thermal power plants in the world, and the biggest in the UK. Drax has converted four out of its 6 coal boilers to biomass combustion withing the past few years, with plans for the conversion of the remaining units. Although Drax has established secondary application for its coal ash; the processing and management of its biomass counterpart has proved to be an existing challenge due to the distinctly different properties of biomass ash compared to that of coal (i.e. elevated alkaline/alkali-earth metal content), hence, an immediate need for effective management of this potentially hazardous solid waste. Preparing efficient yet cost-effective adsorbents from this waste stream could be a practically feasible way to simultaneously mitigate climate change (alongside ash-associated environmental concerns) and decrease the operational expenses.

For cost-effective production of a sorbent from bottom ash (BA), the base-carbon has to be first extracted from the waste source and then its properties have to be enhanced and optimised to maximise the efficiency of the material and the efficacy of production. Physical activation is often employed as a porosity development technique due to its cost-effectiveness and eco-friendliness (Li *et al.*, 2021) as the absence of chemical activating agents (e.g. $ZnCl_2$, KOH and etc.) generally would result in a lower cost, and the avoidance of secondary waste generation (Gorbounov, Petrovic, *et al.*, 2022). This method subjects the virgin carbon to a thermal treatment under a flow of gas to promote porosity development by widening or unblocking the existing pores, in turn leading to a higher gas adsorption capacity (Ketabchi *et al.*, 2023). However, many factors are at play in this process, hence, identification of the "key-players" is imperative for production of the optimum activated carbon (AC).

In order to facilitate an understanding of the main factors and their interactions on the CO_2 uptake, as well as to produce an efficient yet cost-effective adsorbent in this work, we have first extracted the carbon from the BA *via* a one-step direct process, then analysed the resulting virgin material as a potential adsorbent for carbon capture. Afterwards, we have conducted an initial screening study, followed by two separate central composite experimental designs (CCD) to evaluate different activation conditions and their impacts on the resulting sorbent. These design of experiment (DoE) frameworks allowed for efficient data collection and provided valuable insight into the process, whilst simultaneously saving time and resources. The gathered data was also analysed and optimised *via* statistical techniques to achieve the optimum point with maximising the CO_2 capture capacity and the AC yield simultaneously.

2. Materials and Methodology

2.1. Extraction and Preparation of Virgin Carbon

An industrial-grade biomass combustion bottom ash, collected from Drax power plant in Selby, UK, was used as the adsorbent precursor in this work. This waste material was then dried for 12 hours at 110 °C in an oven (Fisher Scientific 825F) as described in our previous work (Gorbounov *et al.*, 2021). The resulting dry BA was then ground in a lab-scale ball mill (Capco Ball Mill Model 2) in two separate batches: crude and then fine grinding (1 L and 0.5 L jars, respectively, each with its appropriate loading/charge). The milling of each batch was carried out for an hour; however, the crude batch was milled at approximately 120 rpm, whereas the fine grinding occurred at nearly 140 rpm. The obtained ground BA was then manually sieved through standard sieves (aperture in the range of 0.1 – 1.4 mm) to extract a desired carbonaceous fraction. The resulting fraction was labelled as BA-100-P (i.e. Bottom Ash – 100 μm – Passed *through the sieve*). The described preparation procedure yielded between 4 – 11% of BA-100-P depending on the composition of the raw BA.

2.2. Preparation of Activated Carbon

The activation campaigns consisted of two separate steps. First a Taguchi-based L18 orthogonal array was used as a tool for a screening study leading to identification of the most important factors impacting the CO_2 adsorption capacity of the sorbent. Then two smaller CCDs were deployed based on the most impactful parameters to develop the database for optimisation of both the yield and the CO_2 uptake capacity of the sample *via* Response Surface Methodology (RSM). Minitab (version 18) was used for the statistical analyses and the generation of the DoE matrices.

The experimental campaign (i.e. activation) was conducted in an insulated tube furnace (Carbolite Gero TF1 12) by placing approximately 0.2 – 0.4 g of the virgin BA-carbon (i.e. BA-100-P) into the centre of the Inconel tube and allowing the selected gas to pass over the material at a prescribed flow rate. The tube was insulated to minimise the temperature gradient. The activation temperature (T_{act}) was achieved using the given ramping rate (RR) in the respective experimental run as well as the activation time, (τ_{act}), desired flow rate (FR) and activating gas itself for that particular experiment. Once the thermal treatment was complete, the sample was left in the tube furnace to cool down to ambient temperature under the same gas and FR used for the respective activation run.

2.3. Sorbent Characterisation

The properties of the investigated materials were analysed *via* thermogravimetric analysis – TGA (Mettler Toledo TGA 2), Scanning Electron Microscopy/Energy Dispersive X-ray Spectroscopy (JOEL IT200), as well as Fourier- Transform Infrared (Perkin Elmer Spectrum One) and Raman (Renishaw Invia Raman Spectroscope) Spectroscopies. The porous surface area (S_{BET}) was obtained following the Brunauer – Emmett –Teller method (Brunauer, Emmett and Teller, 1938) using a 3P Meso 222 Analyser under pure N_2 at 77 K. Prior to this, the samples were degassed at 200 °C for 6 hours with a ramping rate of 15 °C/min. Further, the pore diameters were estimated according to the Barrett-Joyner-Halenda (BJH) method, whereas the microporosity was assessed using the t-plot method.

The Scanning Electron Microscopy/Energy Dispersive X-ray Spectroscopy (SEM/EDS) was carried out without gold-coating, due to the conductive nature of the carbons.

The Fourier- Transform Infrared Spectroscopy (FTIR) measurements were acquired between 4000 and 600 cm^{-1} and with a resolution of 4 cm^{-1}. The spectra were collected following the Attenuated Total Reflection (ATR) method to minimise the use of KBr, hence the prominence of peaks associated with the highly hygroscopic nature of potassium bromide. Additionally, Raman Spectroscopy (at the wavelength of 514 nm) was utilised as a complementary analysis technique in order to reveal the hybridisation state of the carbonaceous framework.

Proximate Analysis was conducted according to the programme described in (ASTM, 2013); however, the analysis was conducted on TGA (using alumina crucibles) to allow for constant recording of mass. Such approach has been previously shown to be effective in the literature (Rashidi *et al.*, 2012; Torquato *et al.*, 2017; Yaumi, Bakar and Hameed, 2018), hence our adaptation in this work.

Ultimate Analysis was carried out using a Flash 2000 Organic Elemental Analyzer (Thermo Scientific) with acetanilide as the standard.

2.3.1. Adsorption Experiments

The sorption properties were analysed *via* TGA studies, evaluating the impact of adsorption temperature (25, 50 and 75 °C) under a fixed volumetric FR (50 mL/min) of pure CO_2. The uptake was measured over a period of 30 min. Prior to the adsorption segment, the sample was purged with 50 mL/min of N_2 at 150 °C to remove moisture alongside other species adsorbed from ambient air. Both gases were acquired from BOC and were of high purity (i.e. N4.8 for nitrogen and N2.8 for carbon dioxide).

Additionally, a commercial AC (Sigma Aldrich, CAS 7440-44-0) has been used as the material for comparison.

3. Results and Discussions

3.1. Activation and Optimisation Campaigns

A mixed level L18 Taguchi orthogonal matrix was developed in order to evaluate the impact of 5 different factors at various levels (the categorical variables were studied at 2 levels, whereas the quantitative parameters had 3 levels each) as shown in Table 1.

Table 1. Factors and their respective levels evaluated within the L18 mixed level Taguchi orthogonal array.

Factors	Levels		
Gas	CO_2	N_2	
Time (τ_{act}), min	30	50	70
Temperature (T_{act}), °C	700	800	900
Flow Rate (FR), mL/min	100	200	300
Ramp Rate (RR), °C/min	5	15	25

The results of this pseudo-screening study have been analysed *via* analysis of variance (ANOVA) using the CO_2 uptake as the response (Table 2).

Table 2. Results of statistical analysis of the screening experimental campaign.

Factors	F-Value	p-Value	Significance
Gas	55.2	0	1
Time (τ_{act}), min	1.31	0.322	5
Temperature (T_{act}), °C	22.46	0.001	2
Flow Rate (FR), mL/min	2.38	0.154	4
Ramp Rate (RR), °C/min	4.77	0.043	3

Following the F and p-values derived from the model (regression coefficient $R^2 = 0.936$), the conclusion on the significance of each factor has been made. The results showed that the activation time was not statistically significant and had the least impact on the adsorption capacity of the produced material. This phenomenon was attributed to the fact that a low ramping rate would inherently increase the time during which the carbon has been subjected to thermal treatment. Thus, resulting in the latter parameter having a stronger effect on the resulting outcome. This finding also suggests that the pore-unclogging (i.e. the release of volatile organic compounds - VOCs) - which is proposed to occur during the activation of BA-100-P - starts at temperatures below 700 °C, hence, exacerbating the impact of the ramping rate, whilst simultaneously diminishing the importance of the holding time at the activation (i.e. maximum) temperature. Furthermore, with CO_2 activation, the same temperature is the point after which the *reverse* Boudouard reaction (Dai *et al.*, 2021) - i.e. the proposed mechanism for CO_2 activation - starts favouring CO production, thus alleviating some surface carbon atoms and generating porosity.

Boudouard reaction $2CO \rightleftharpoons CO_2 + C$ $(\Delta H_{298\,K} = 172\ kJ/mol)$ *Eq. 1*

Within that, however, the process entails formation of surface oxides, labelled as C(O), which may decompose in form of carbon monoxide, thus closer representing the reverse Boudouard reaction. Alternatively, the surface oxide complex might stabilise on the carbon surface, producing an oxygen-containing surface functional group (Marsh and Rodríguez-Reinoso, 2006).

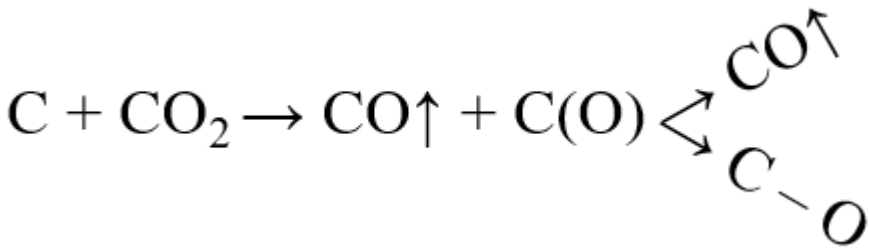

Figure 2. Potential reaction mechanism of CO_2 activation.

This functionality may or may not be beneficial for the adsorption due to changes of the electrostatic potential of the surface or by blocking access to micropores. A similar optut might occur if the carbon active site would adsorb a produced CO molecule. This would lead to a C(CO) complex which could, again, either, decompose or persist on the surface retarding gasification of the rest of the carbon framework (Sajjadi, Chen and Egiebor, 2019). These many variations could stem from a number of potetial inputs. For instance, the organic precursor might be isotropic or anisotropic, whereas the produced virgin carbon might be graphitisible or non-graphitisible. Moreover, the ash impurities could also impact the output, since they could act as a catalyst to a given process (or pathway). This would in-turn raise question of the size of the catalyst particles, their nature and composition as well as distribution within the carbonacous material. This phenomenon is known to impact the process of activation with CO_2 (Marsh and Rodríguez-Reinoso, 2006). Additional variation might be assosiated with the place where these reactions occur i.e. between basal planes of graphene layers or reacting with the edge carbon atoms. Finally, the type of formed surface complexes also plays a crucial role.

Another noteworthy point is the lack of CO_2 uptake for the activated carbon (AC) produced at the harshest activation temperature using CO_2 as the activating agent. Regardless of other studied parameters and their levels, the samples activated at 900 °C had a miniscule yield and were visibly different (grey powder) from others (black powder) as shown in Figure 3, hence leading to an assumption that these samples are not of carbonaceous nature but rather ash. The material shown in Figure 3b is believed to be produced from an "extreme extent" of the reverse Boudouard reaction leading to a complete loss of carbon from the sample during the process. The proposed logic was further confirmed *via* SEM/EDS and proximate analysis proving the "ashy" nature of the samples. Additionally, the samples activated at 800 °C with CO_2 have also underperformed (presumably due to creation of larger micropores by pore widening rendering them less favourable for CO_2 adsorption) and had a low AC yield. Therefore, for physical activation with CO_2, temperatures below 900 °C (or even 800 °C) were found to produce sorbents better suited for CO_2 adsorption.

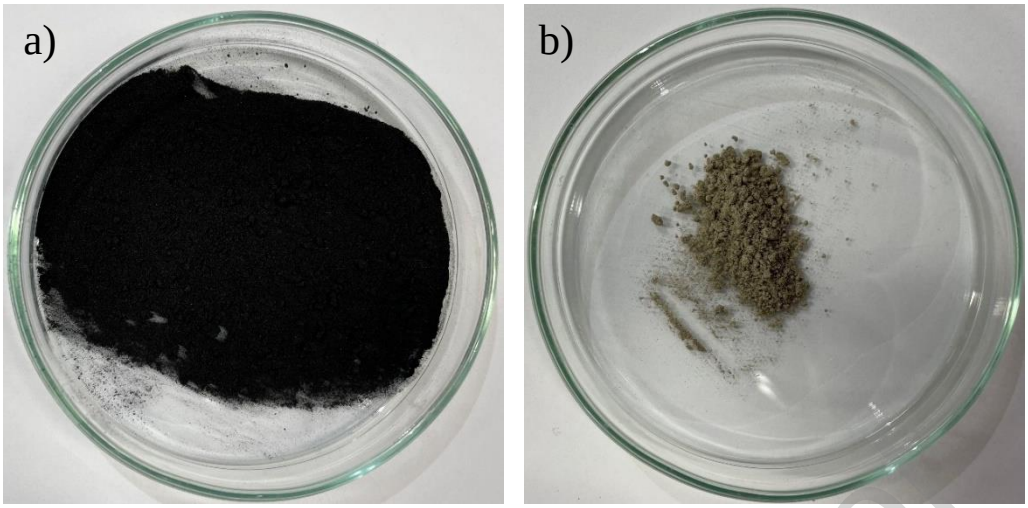

Figure 3. Activated carbon samples activated at 700 °C (a) and at 900 °C (b).

Following the Taguchi screening campaign, the statistically significant (at the evaluated levels) parameters have been investigated further with two separate CCDs. This particular DoE framework has been employed due to its superior ability to estimate any potential "curvature" as well as to "peek" outside of the lower boundary of the activation temperature (due to the positioning of the axial/star points) (Gorbounov, Taylor, *et al.*, 2022). The latter reason is of utter importance as this could potentially assist in increasing the adsorbent's uptake, whilst minimising the energy requirement for thermal treatment. Consequently, two separate CCDs with the same conditions for each of the activating gases were created with the statistically significant parameters being varied and the others being kept at their lowest value (τ_{act} = 30 min, FR = 100 mL/min) in the interests of green chemistry. Further, this design incorporated three repetitions at the "centre point" conditions to prove repeatability of the results. A visualisation of the new design space is given in Figure 4.

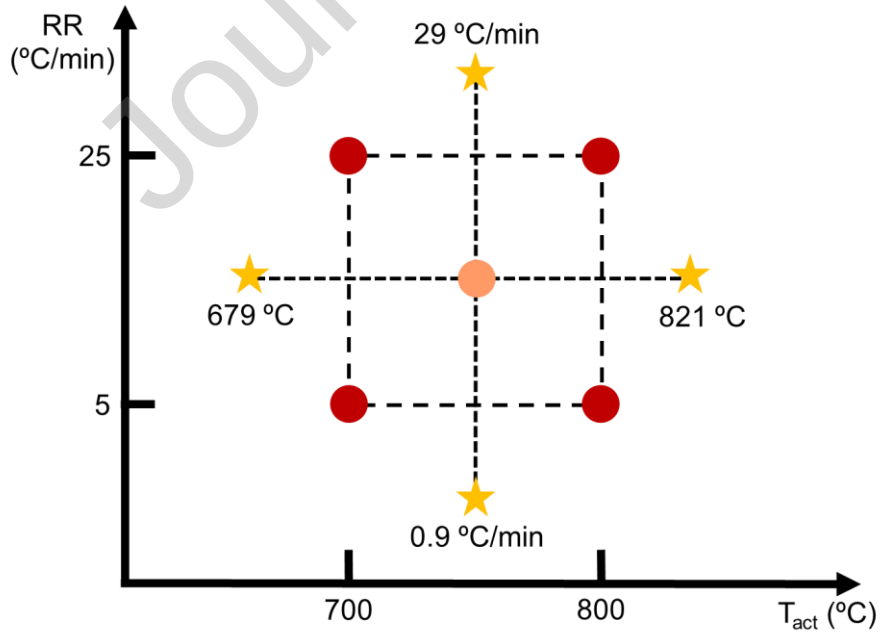

Figure 4. The design space used for the optimisation of BA-100-P activation with CO_2 and N_2.

Following the CCD experimental campaigns, the outputs were analysed in a similar fashion to the screening study. Identification of the optimum points has been done utilising Minitab and the RSM results of the model (R^2 = 98%) evaluating the CO_2 activation experiments are presented in Figure 5 in from of a contour plot.

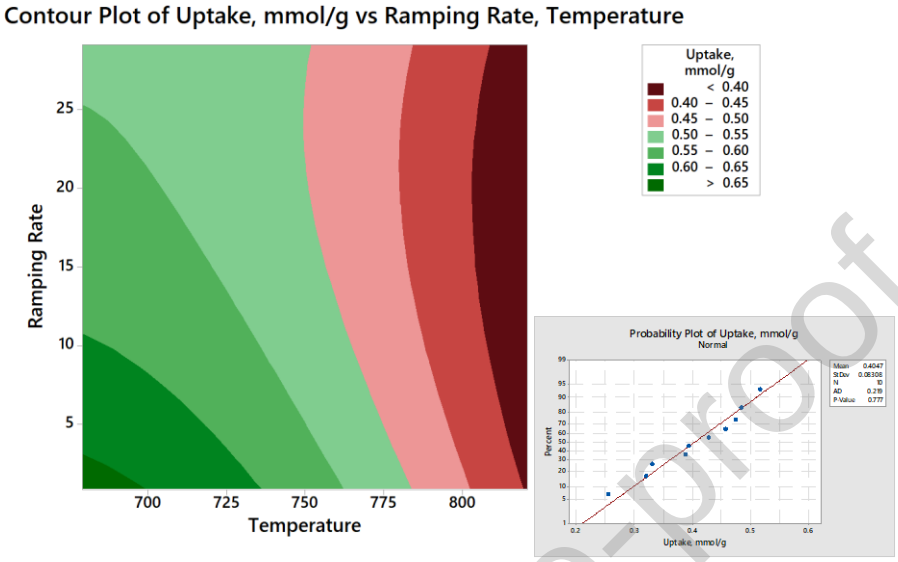

Figure 5. Contour plot of CO_2 uptake vs RR and T_{act} for the activation with CO_2 as well as the normality plot as insert (bottom right corner).

The trend of enhanced adsorption approaching the bottom left corner of Figure 5 is quite evident, suggesting the activation conditions for maximising uptake to lie outside of the original design space at lower levels. This is down to the fact that pore unclogging without damage to the morphology of the surface is proposed to occur at $T_{act} \leq 700$ ºC. Above this level, the Boudouard reaction equilibrium is shifted towards CO production (Sajjadi, Chen and Egiebor, 2019) , hence, increasingly affecting the carbon. At first, in the temperature region of ~ 700 – 750 ºC, a minor decrease in yield and uptake of the final product (due to a degree of pore-widening) is observed. This is then followed by a pronounced drop in both of the dependent variables, i.e. uptake and yield, (~ 750 – 800 ºC). Then at temperatures of approximately 800 – 850 ºC, severe damage to the pore structure causes a minute CO_2 adsorption capacity. Finally, complete oxidative degradation of the carbon is observed (~ 850 – 900 ºC), resulting in a change of physico-chemical properties of the material, leading to the absence of any CO_2 uptake and a miniscule product yield (as noted previously for Figure 3). As such, the statistical significance of both of the studied parameters as well as their linear interaction is to be expected (F and p-values can be found in Table 3).

Table 3. Results of the ANOVA for the CO_2 activation campaign.

Source	F-Value	p-Value
Model	39.52	0.002
Linear	89.5	0
Temperature	161.98	0
Ramping Rate	17.01	0.015
Square	8.34	0.037
Temperature*Temperature	6.93	0.058
Ramping Rate*Ramping Rate	2.87	0.166

2-Way Interaction	1.92	0.238
Temperature*Ramping Rate	1.92	0.238

The model was validated *via* equally weighted dual response optimisation, maximising yield and uptake. Following response optimisation, the sample activated at 679 °C with an RR of 0.9 °C/min adsorbed an increased amount of CO_2 (0.689 mmol/g) under a pure flow of CO_2 and 50 °C, and showed a good product yield of 62.3%. Nevertheless, the trend depicted in the contour plots suggests a potential for a further rise in capture capacity at T_{act} lower than 679 °C for this BA-derived carbon. The nitrogen activation experimental campaigns as well as response optimisation, however, did not suggest a lower activation temperature.

Activation under N_2 can be somewhat equivocated to conventional pyrolysis in terms of lack of an oxidising atmosphere. During this process the major changes happen at temperatures lower than the ones evaluated here. At 300 – 500 °C dehydration occurs, which is evidenced by the loss of elemental O and H (Keiluweit *et al.*, 2010), thus, eliminating hydroxyl groups. The alcohol surface functional groups may also convert to C=O in the carboxylation reactions at temperatures below 500 °C. Surpassing this threshold; however, the carboxyl functionalities become consumed *via* dihydroxylation and/or dehydrogenation reactions (Harvey *et al.*, 2012). These processes result in evolution of volatile organic compounds in form of various decomposition products. Further, at temperatures of about 900 °C, shrinkage of the micropore structures (hence, loss of surface area) has been previously reported in the literature, and attributed to loss of free sites and defects as a result of high-temperature annealing (Antal and Grønli, 2003). The inert atmosphere acts as a carrier gas to releave the evolved volatile species from the surface of the carbon, thus preventing their recondensation throughout the process. The constant flow of the carrier gas (i.e. nitrogen in our study) facilitates the mass transfer of the decomposed products during the thermal treatment of the char (i.e. from the space immediately above the char's surface to the bulk of the carrier gas) and thus, entertaining a more efficient overall process. The contour plots (R^2 = 91.5%) of the CO_2 adsorption uptake versus T_{act} and RR for the N_2 activation campaign are shown in Figure 6.

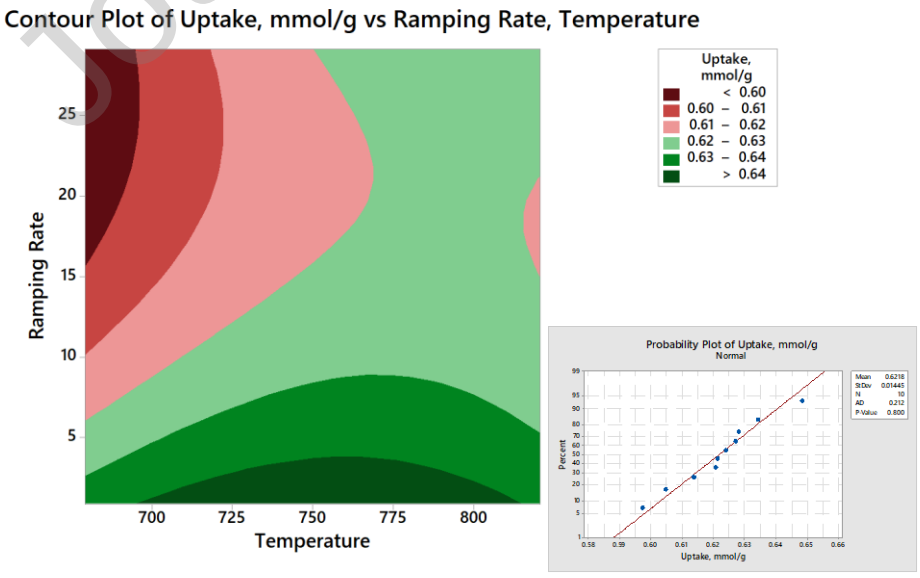

Figure 6. Contour plot of CO_2 uptake vs RR and T_{act} for the activation with N_2 as well as the normality plot as insert (bottom right corner).

As evident from Figure 6, curvilinear relationships exist within the design space. Furthermore, both RR and T_{act} as well as their linear interaction were found to be statistically significant (F and p-values are given in Table 4).

Table 4. Results of the ANOVA for the N_2 activation campaign.

Source	F-Value	p-Value
Model	8.63	0.029
Linear	13.98	0.016
Temperature	9.03	0.04
Ramping Rate	18.92	0.012
Square	6.77	0.052
Temperature*Temperature	3.03	0.157
Ramping Rate*Ramping Rate	4.77	0.094
2-Way Interaction	1.63	0.271
Temperature*Ramping Rate	1.63	0.271

Additionally, the grouping of both of the quadratic terms due to its p-value of 0.052 could also be a potential contributor, and to some extent accounting for the non-linearity of the response surface in Figure 6. Nevertheless, the proposed optimum activation conditions were suggested to be 748 °C and 0.9 °C/min.

Both of the activation campaigns resulted in an increase of the adsorption capacity compared to the virgin carbon. In addition, N_2 activation yielded very similar results with the CO_2-activated AC, both in terms of uptake and product yield. However, the CO_2-activated sample was deemed to have more favourable properties (lesser energy requirement for activation due to a lower T_{act} as well as potential for its further reduction) and was chosen for characterisation and analysis under the alias of AC-Opt.

3.2. Material Characterisation

This section will address the physicochemical properties of the virgin carbon (BA-100-P) and the produced optimum AC (AC-Opt). In contrast to other waste-derived carbonaceous adsorbents, BA-100-P does not need to be fundamentally carbonised/pyrolysed prior to activation (due to partial carbonisation upon combustion). This would potentially lead to a significant reduction in the overall costs associated with the preparation of the final sorbents (i.e. a less energy intensive process).

3.2.1. Scanning Electron Microscopy/Energy Dispersive X-ray Spectroscopy

The surface morphology as well as the elemental composition of the produced materials were analysed *via* SEM/EDS (Figure 7 andFigure 8).

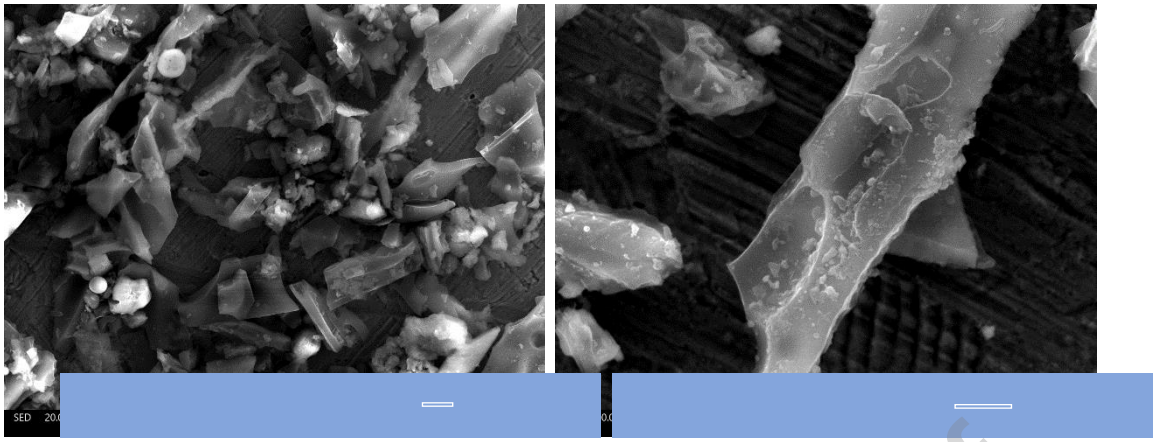

Figure 7. SEM images of a) virgin BA-100-P and b) AC-Opt.

BA-100-P, as can be inferred from Figure 7a, is a heterogenous collection of crystalline and amorphous carbon with inclusion of spherical particulates of aluminosilicate origin. Such results are to be expected and are in agreement with our earlier primary *proof-of-concept* study (Gorbounov *et al.*, 2021). Similarly, the elemental composition of the produced material is also in line with the previous work, showing Ca to be the most prevalent metallic element (constituting over 1.5 wt%) followed by a lesser amount of both Si and Al (0.5 wt% each). The spectrum of the EDS analysis (Figure 8a) can be found below.

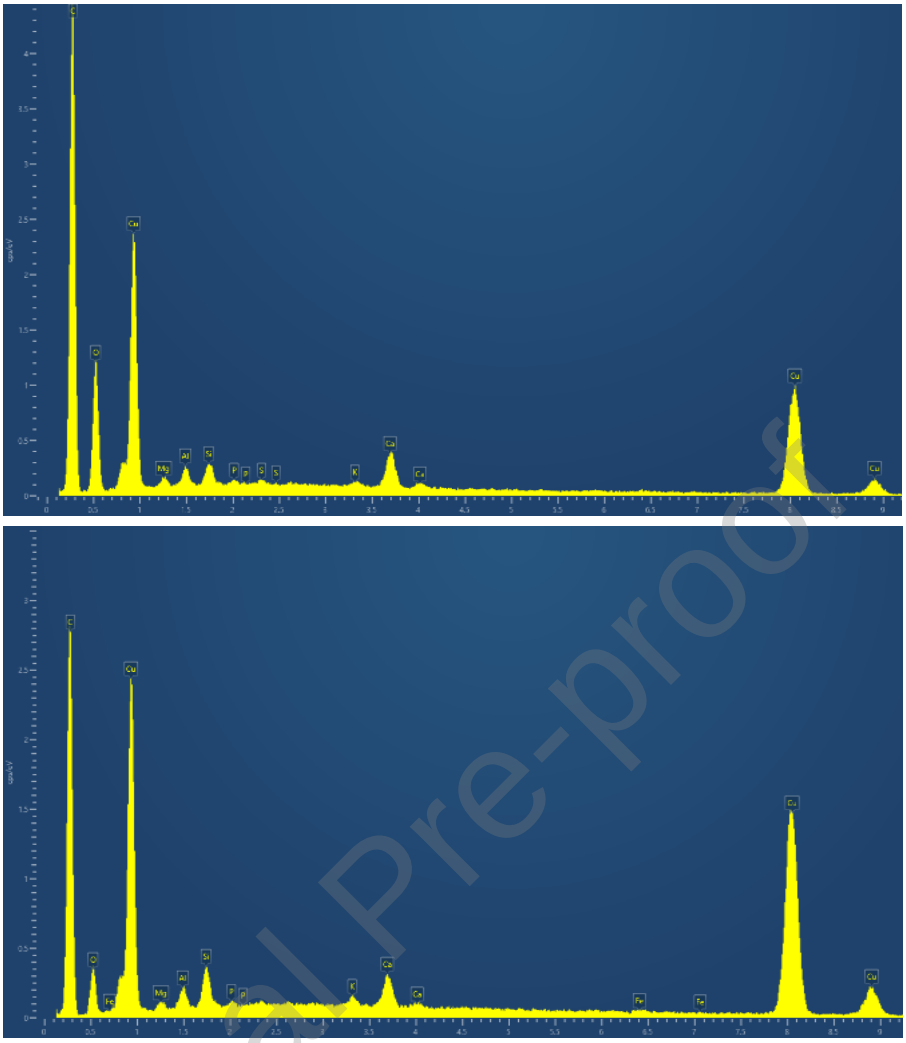

Figure 8. EDS spectra of a) virgin BA-100-P and b) AC-Opt.

The morphology of the studied samples is quite similar However, AC-Opt shows a more prominently developed surface heterogeneity (Figure 7b). Additionally, the elemental composition has changed slightly as evident by a decreased elemental C peak (Figure 8b). This is to be expected and is attributed to the loss of carbonaceous species (i.e. burn-off) during the activation process. It is noteworthy, that the prominent Cu peaks shown in Figure 8 are associated with the background as for analysis the samples were placed onto copper plates.

3.2.2. Ultimate Analysis

CHN-analysis, otherwise known as ultimate analysis, has corroborated the EDS results further confirming successful carbon extraction from the waste stream. BA-100-P was shown to contain approximately 60% of elemental C, just over 3% of elemental hydrogen and less than 0.5% of N. The ultimate analysis results for AC-Opt are in agreement with the data collected from other analytical techniques. The bulk of the activated sample has a lower carbon content than the virgin sample (namely, 54.5%) as well as less hydrogen and nitrogen by weight. The decreased values can be linked to the loss of carbonaceous matter upon thermal treatment. The results of the analysis can also be found in Table 5.

Table 5. Ultimate analysis results – BA-100-P and AC-Opt.

Sample name	Element	Weight %
BA-100-P	C	60.07
	H	3.16
	N	0.42
AC-Opt	C	54.47
	H	1.00
	N	0.26

It should be noted that the EDS results account for the surface elements, whereas ultimate analysis measures the bulk content of the described above elements, leading to some minor discrepancies.

3.2.3. Proximate Analysis

The sample has been further evaluated *via* proximate analysis (ASTM, 2013) to quantify the amounts of ash impurities in the proposed sorbent alongside the fixed and the volatile organic compounds (VOC) as well as moisture content with the results shown in Table 6.

Table 6. Proximate Analysis Results.

Sample name	Moisture, wt%	VOC, wt%	Fixed C, wt%	Ash, wt%
BA-100-P	9	30	37	24
AC-Opt	1.5	7	49	42.5
Commercial AC	5	4	85	6

The trends observed further corroborate the release of volatile compounds from the virgin carbon upon activation.

3.2.4. Spectroscopic Analysis

3.2.4.1. Fourier- Transform Infrared Spectroscopy

Both BA-100-P and AC-Opt were analysed *via* FTIR with the results presented in Figure 9.

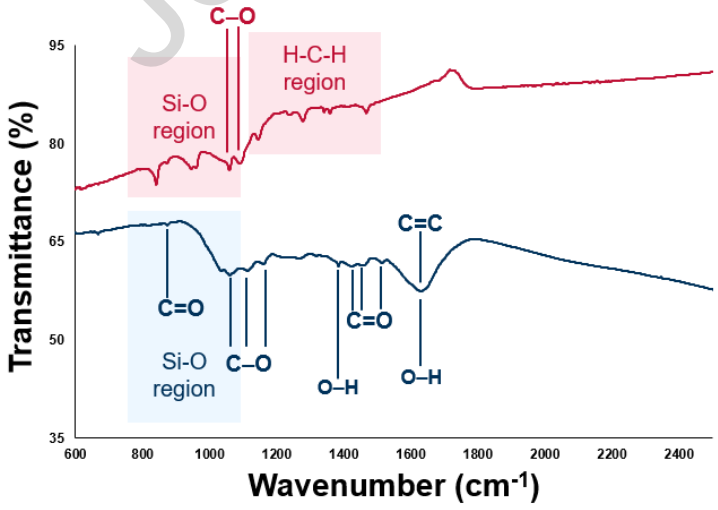

Figure 9. Infrared spectra of BA-100-P (bottom blue line) and AC-Opt (top red line).

The produced spectra are quite vivid and contain a variety of different bonds; however, the changes upon activation are nevertheless clear. For instance, the spectrum of BA-100-P (blue line in Figure 9) contains the bands at wavenumbers of 873, 1425, 1455 and 1515 cm^{-1}. They can all be attributed to various vibrational modes of the C=O bonds present in different configurations (mainly carbonyl functionalities on the carbon surface and metal carbonates) (Mozgawa *et al.*, 2014; Chindaprasirt and Rattanasak, 2019; Assad Munawar *et al.*, 2021). Additionally, a cluster of peaks around the 1000 – 1100 region (namely, 1036, 1062 and 1114 cm^{-1}) are believed to represent asymmetric stretching vibrations of the Si-O bonds present in all of the aluminosilicate impurities (Mozgawa *et al.*, 2014). However, myriad factors impact the final positioning of the band on the spectrum. Presence of Al within the framework will cause the wavenumber to decrease (also known as a "red shift") when compared to pure Si-O-Si bonding. Moreover, the amorphous nature of the particles may also lead to a lower position of the peak when comparing to the pure crystalline quartz. Additionally, the band at 1062 cm^{-1} might be associated with C-O bonds in epoxy groups (Somanathan *et al.*, 2015), whilst the 1114 cm^{-1} (and the 1160 cm^{-1}) peak could represent the C-O stretching vibrations found in graphene oxides (Pham *et al.*, 2011; Sudesh *et al.*, 2013). Another bond often present in graphite, graphene and graphene oxides (i.e. the aromatic C=C stretch) presents itself at around 1634 cm^{-1} (Pham *et al.*, 2011). This wavenumber, however, could also be attributed to the bending vibrations of the hydroxyl functionality (Mozgawa *et al.*, 2014) with the stretching vibrations positioned at 1383 cm^{-1} (Raizada *et al.*, 2017). Another peak that is representative of the O-H bond (not shown in Figure 9) is present around 3450 cm^{-1} (Pham *et al.*, 2011; Raizada *et al.*, 2017; Gómez *et al.*, 2020). Furthermore, the band at 2355 cm^{-1} is descriptive of the CO_2 in the background of the scan (Derrick, Stulik and Landry, 1999), whereas the peaks at 2857 and 2930 cm^{-1} can be ascribed to the aliphatic C-H bonds (Pham *et al.*, 2011; Sudesh *et al.*, 2013). These last 4 bands have been eliminated from Figure 9 to enhance the visibility of changes upon activation.

The spectrum of AC-Opt (shown in red in Figure 9), clearly depicts elimination of many surface functionalities upon heat treatment. This is to be expected as activation with CO_2 is known to eliminate C=O bonds as well as hydroxyl groups (Sajjadi, Chen and Egiebor, 2019). Instead, the AC-Opt spectrum contains various vibrations (1240, 1279, 1342, 1360 and 1467 cm^{-1}) of the methylene groups with the latter wavenumber depicting in-plane bending (scissoring) of CH_2 (Derrick, Stulik and Landry, 1999). The band at 1360 cm^{-1} could, as with the virgin carbon, be associated with the hydroxyl functionality but probably represents the symmetric bending of CH_3 (Derrick, Stulik and Landry, 1999). This splitting might be caused by the presence of semi-crystalline strictures within the sample. However, not all functionalities have been lost during the thermal treatment, with the C-O graphitic stretch present at 1147 cm^{-1} (Pham *et al.*, 2011; Sudesh *et al.*, 2013) and the epoxy C-O band at 1060 cm^{-1} (Somanathan *et al.*, 2015). As with the virgin C, a cluster of peaks can be observed in the Si-O region (namely 946, 961, 1060 and 1090 cm^{-1}). The minor shifts in the wavenumbers upon activation could be a sign of either Si-O bonds undergoing transformations, or of the inherent structural disorder of the produced AC and/or virgin carbon precursor.

3.2.4.2. Raman Spectroscopy

Raman spectroscopy is a widely used complementary technique to FTIR, that could be used to analyse the crystallinity and/or presence of defect on the surface of a carbonaceous

adsorbent. As can be seen in Figure 10, the peaks at approximately 1353 and 1585 cm^{-1} are ascribed to the D (generally assigned to the defects present in the structure and/or disordered/sp^3-hybridised carbon atoms as well as the edges of graphene sheets) and G-band carbons (describing the graphitic carbons in sp^2 hybridisation state), respectively (Somanathan *et al.*, 2015). Both samples clearly present the aforementioned peaks, with I_D/I_G ratios of 0.81 for AC-Opt and 0.73 for the virgin BA-100-P. This indicates an increase in defects on the surface of the activated carbon (suggesting a greater degree of heterogeneity) as well as (potentially) partial transformation from sp^2 to sp^3 hybridisation state.

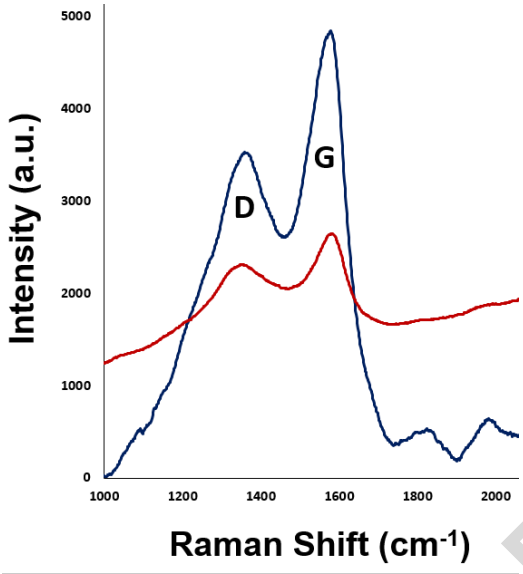

Figure 10. Raman spectra of BA-100-P (blue line) and AC-Opt (red line).

3.2.5. Surface Area Analysis

The BET surface area of the virgin carbon sample was measured and calculated to be 4.6 m^2/g, whereas the activated sample has shown a substantial enhancement in S_{BET}, rising to 248 m^2/g. Further, a significant change in the nature of the samples' surfaces has been observed as can be visualised from Figure 11. Namely, the virgin BA-100-P exhibits a type I physisorption isotherm (following the IUPAC technical report (Thommes *et al.*, 2015)), with a very low plateau. This is, however, to be expected as such isotherms are typical for microporous samples that have a relatively small external surface area (Thommes *et al.*, 2015). Indeed, the t-plot microporous area is 3 m^2/g, constituting ~65% of the surface area. AC-Opt, on the other hand, presents a type IV physisorption isotherm which is characteristic of mesoporous samples (Rouquerol *et al.*, 2013). Similarly to type I, type IV are expected to present a saturation plateau, however, it could be (as is in the case of Figure 11 b) reduced to a simple inflexion point (Rouquerol *et al.*, 2013). Further, a characteristic type H4 hysteresis loop is observed. This phenomenon is often found with micro-mesoporous carbons (Thommes *et al.*, 2015) and is to be expected since approximately 74% of the surface of AC-Opt is microporous (t-plot microporous area of 183 m^2/g).

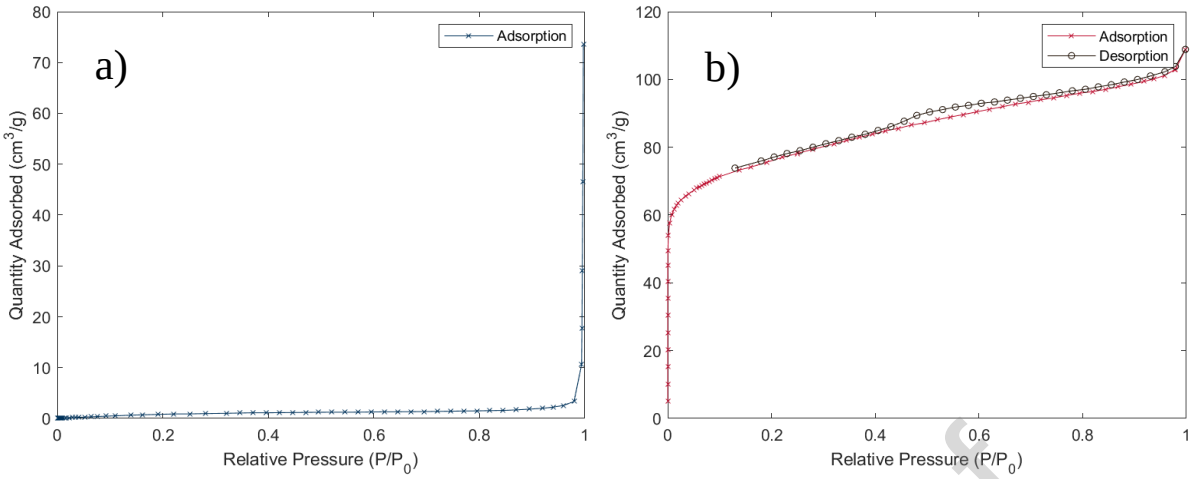

Figure 11. BET Surface area of the evaluated materials, namely a) BA-100-P and b) AC-Opt.

Additionally, the t-plot micropore volume has also undergone a dramatic change: rising from 0.00087 cm3/g to 0.0936 cm3/g for BA-100-P and AC-Opt, respectively. Similarly, the pore diameters have also changed drastically, though following the opposite trend. The virgin carbon (according to the BJH desorption average pore diameter) has the pore size of 14 nm, which upon activation has shrunk down to 3.7 nm. This is to be expected as the produced microporosity would skew the average pore diameter to the lower end, whilst the presence of a hysteresis loop suggests some pores to be larger than ~4 nm (Thommes et al., 2015). This shift towards a higher degree of microporosity can also be visualised from the pore size distribution plots in Figure 12, especially when examining the pore volumes.

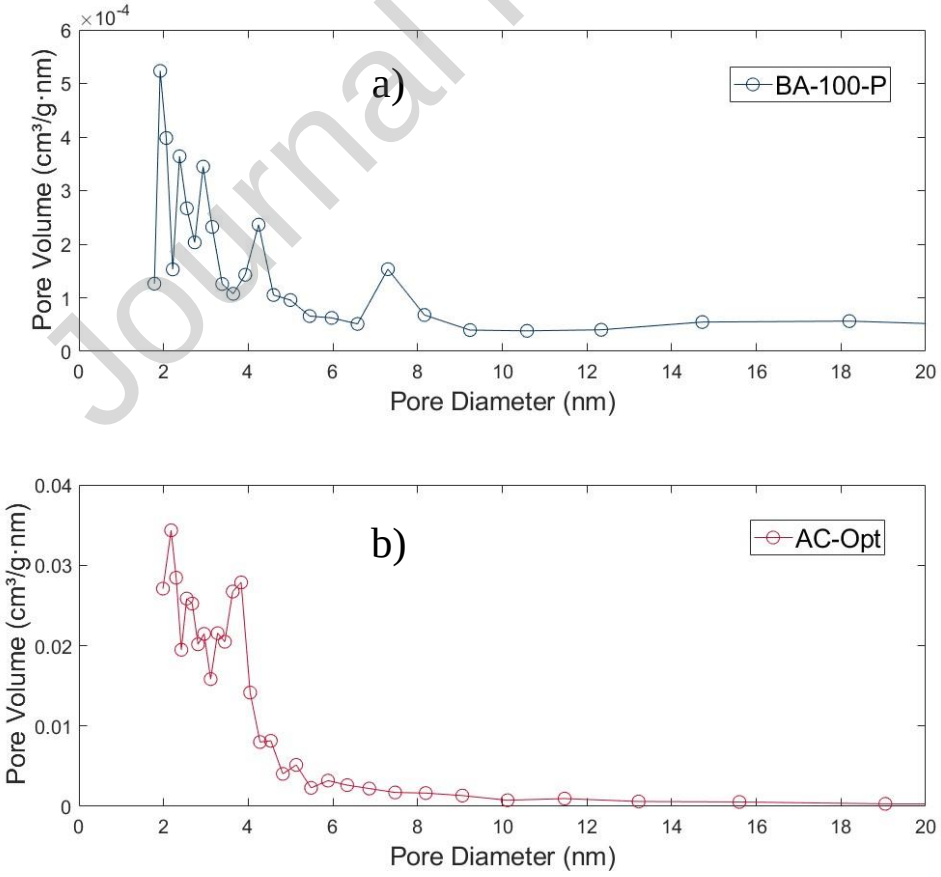

Figure 12. Pore size distribution plots a) BA-100-P in blue and b) AC-Opt in red.

Evidently, extraction (itself or followed by activation with CO_2) of biomass combustion bottom ash-derived carbons results in highly micro-/mesoporous adsorbents. However, apart from prominent surface characteristics such materials should also have a high affinity towards CO_2.

3.2.6. CO_2 Adsorption Experiments

The equilibrium capacity of the produced materials can be used to evaluate the efficacy of activation. However, this criterion alone cannot determine the applicability of the material.

3.2.6.1. Adsorption Kinetics

Adsorption kinetics have to also be evaluated when considering wide industrial implementation. Therefore, the produced adsorption curves have been analysed to investigate the sorption kinetics. Classically, two kinetic models are often proposed to describe the kinetics of physisorption, namely, pseudo-second order (PSO) and pseudo-first order (PFO). Both models are presented below:

PFO $$\boldsymbol{F = q_t/q_e = 1 - e^{-K_1 t}} \quad \textit{Eq. 2}$$

PSO $$\boldsymbol{F = K_2^* t/(1 + K_2^* t)} \quad \textit{Eq. 3}$$

where, F is the fractional uptake, which is defined as q_t (i.e. adsorption capacity at time t) divided by q_e (the equilibrium uptake). K_1 and K_2 are the kinetic constants of the respective equations; further, K_2^* is defined as q_e multiplied by K_2.

An overwhelming majority of published literature tends to favour the former over the latter due to a number of issues, which arise as a result of the employed mathematical technique: a) use of linear regression, b) inconsistent scales for comparison of models, c) excessive use of data points close/at equilibrium, d) use of both the regression coefficient (R^2) fit and the ability to approximate the equilibrium capacity as the deciding factor. These aspects affect the accuracy of the modelling leading to a bias towards the PSO. These issues have been described eloquently in the literature and in this work we have adopted the improved methodology as per (Simonin, 2016). Nevertheless, PFO assumes the sorption rate to be proportional to the number of free adsorption sites, whereas PSO is proportional to the square number of sites available (Singh and Kumar, 2016). As a result, the PFO kinetic model is not strongly dependent on the adsorption sites and may be more applicable to materials/processes where few active sites exist on the adsorbent surface (Wang and Guo, 2020). Furthermore, if PFO fails to adequately fit the experimental data, adsorption is believed not to be diffusion-controlled (Masoudi Soltani *et al.*, 2015) since the rate limiting step for this kinetic model is external/internal diffusion (Wang and Guo, 2020). PSO, on the other hand, is often ascribed to chemisorption (Masoudi Soltani *et al.*, 2015). This notion could stem from the fact that the pseudo-second order kinetic model relies much more heavily (in comparison to PFO) on the presence of active adsorption sites. These include surface functional groups (that increase a material's affinity towards CO_2 (Petrovic, Gorbounov and Masoudi Soltani, 2021)) which tend to act as the binding sites thus, suggesting chemisorption. Further, the PSO model could also represent conditions of low adsorbate concentrations and/or the final stages of adsorption, whereas PFO might be representative of the opposite conditions, namely, few active adsorption sites, high concentrations and initial stages of adsorption (Wang and Guo, 2020).

Apart from evaluating the kinetic models on the same scale and *via* non-linear regression, the determination of the mathematical models that describe best the experimental data should not

be achieved basing the results exclusively on the regression coefficient. A plethora of error calculation methods and functions exist, however, in this work we have aimed at minimisation of the normalised root mean square error (NRMSE). This function has been adopted as it is non-dimensional, hence allows bigger versatility in application. The formula used for NRMSE calculation is provided below:

$$NRMSE = \sqrt{\frac{\sum_{i=1}^{n}(X_{exp,i} - X_{mod,i})^2}{n}} \Big/ \overline{X_{exp}} \qquad \text{Eq. 4}$$

As such, the evaluated AC fits the PSO model better than the PFO, whereas the virgin carbon behaves the opposite across the evaluated temperatures (Figure 13). This could be attributed to the porosity developed on the activated sample which significantly increases the active and available adsorption sites, leading to an enhanced impact of this mechanism on the process.

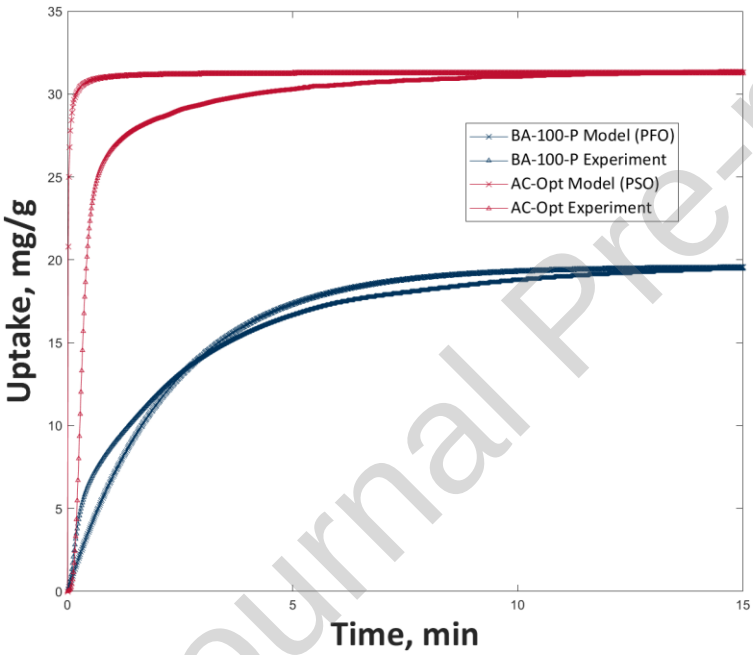

Figure 13. Comparison of experimental data (triangles) and the appropriate kinetic models (crosses) for BA-100-P (bottom blue lines) and AC-Opt (top red lines) at 50 °C, 1 bar with pure CO_2.

The virgin carbon (i.e. BA-100-P), on the other hand, tends to be more accurately represented by the PFO kinetic model. This phenomenon is in agreement with the hypothesis of diffusion-controlled nature of adsorption for the virgin carbon extracted from bottom ash as it possesses fewer free adsorption sites. Additionally, evaluating a commercial AC further corroborates the theory of PSO's stronger dependence on the number of available adsorption sites, as this material also fits the same kinetic model as AC-Opt. These results are shown in Table 7.

Table 7. Adsorption capacity of the produced materials at 1 bar and under pure CO_2.

Sample	Uptake at 25 °C, mmol/g	Uptake at 50 °C, mmol/g	Uptake at 75 °C, mmol/g	Kinetic model	R^2	NRMSE
BA-100-P	0.53	0.340	0.14	PFO	0.957	0.00233

AC-Opt	1.04	0.69	0.43	PSO	0.950	0.00087
Commercial AC	1.23	0.68	0.40	PSO	0.970	0.00096

Table 7 also presents the collected data which shows the temperature-dependant nature of physisorption. Since this process is exothermic, a rise in temperature is leads to a decrease in CO_2 uptake. As expected, all of the evaluated samples behave accordingly. Nevertheless, the proposed optimum activation conditions lead to the adsorption capacity doubling across the investigated temperature range. Additionally, AC-Opt has a comparable uptake to a commercially available analogue, outperforming the alternative material in the appropriate post-combustion carbon capture temperature region (i.e. 40 – 80 °C). It should be noted, however, that the results presented in Table 7 have been acquired *via* TGA studies, which have some limitations, namely, the inability to accurately represent gas-solid contact of a fluidised bed reactor (Raganati, Chirone and Ammendola, 2020) or the obstacles of significant pressure drop in a fixed bed system.

3.2.6.2. Adsorption Isotherms

Another vital aspect of adsorption are the isotherm models. They are paramount for identification of myriad parameters that inform first-principle process models as well as facilitate an understanding of adsorbent properties such as the porous structure, adsorbent surface homogeneity and the capacity, adsorption mechanism and adsorbent-adsorbate interactions (Hossain, Ngo and Guo, 2013; Calzaferri, Gallagher and Brühwiler, 2022; Zhang *et al.*, 2022). Within the abundance of proposed isotherm models, Langmuir and Freundlich isotherms are the most widely used (Masoudi Soltani *et al.*, 2015), whereas Toth isotherm is quite often applied to gas-phase applications as it can overcome some of the limitations of the other two models (Mozaffari Majd *et al.*, 2022).

The Langmuir isotherm model's original purpose was to describe gaseous species being physisorbed on ACs (Vijayaraghavan *et al.*, 2006). This isotherm assumes the adsorbent to possess a flat/smooth energetically homogenous surface (with the adsorption energy being constant regardless of the coverage) and the adsorbate to act an as ideal gas. Additionally, a lack of steric hinderance as well as no migration of the adsorbed species or lateral interactions (neither site-site nor site-adjacent gas molecule) are further assumptions for the Langmuir model. Finally, adsorption is believed to be exclusively monolayer and fully reversible. Therefore, a good fit of this model is often ascribed to chemisorption, which, however, may not always be the case; other parameters (e.g. heat of adsorption) have to be equally considered before coming to such a conclusion, especially accounting for the fact that this isotherm model is often applicable to solid-gas systems that are "weakly" adsorbed. Nevertheless, the Langmuir equation is paramount and fundamental to facilitate the understanding of the adsorption process, and is expressed by:

$$q_e = \frac{q_{max} \times K_L \times P}{1 + K_L \times P} \qquad \textit{Eq. 5}$$

where, q_e is the equilibrium adsorption capacity, mg/g; q_{max} – the maximum adsorption capacity of the material, mg/g; K_L is the Langmuir constant (also known as adsorption affinity factor), 1/bar; P is the adsorbate pressure, bar.

In reality, however, adsorption sites are most probably not equal, with varying surface functional groups (Petrovic, Gorbounov and Masoudi Soltani, 2022) as well as differing degrees of amorphisity/crystallinity. Therefore, in order to overcome the limitations of the original Langmuir isotherm, an extension to this model has been proposed, namely the Multi-site Langmuir adsorption isotherms (in this work, Dual-site (bi-Langmuir) and Triple-site (tri-Langmuir) isotherms have been evaluated). As these models account for gas molecules filling the most favourable adsorption sites first followed by the less favourable, they can be applied to materials with heterogeneous surfaces (Chen, Liu and Dai, 2022a). Applying Multi-site Langmuir isotherms also significantly benefits from a large number of independent fitting parameters (Chen, Liu and Dai, 2022b). Further, these models can account for multiple adsorption mechanisms and are described as:

$$q_e = \sum_{i=1}^{z} \frac{q_{max(i)} \times K_{L(i)} \times P}{1 + K_{L(i)} \times P} \qquad \textit{Eq. 6}$$

where, q_e is the equilibrium adsorption capacity, mg/g; $q_{max(i)}$ – the maximum adsorption capacity at the appropriate site, mg/g; $K_{L(i)}$ are the Langmuir constants (as the adsorption affinities), 1/bar; P is the adsorbate pressure, bar.

Both classical (single-site) Langmuir and Multi-site Langmuir have been extensively applied to various systems within the context of CO_2 adsorption (Ammendola, Raganati and Chirone, 2017; Guarín Romero, Moreno-Piraján and Giraldo Gutierrez, 2018; Kiełbasa *et al.*, 2021) as well as other adsorbates (Adamczuk and Kołodyńska, 2015; Masoudi Soltani *et al.*, 2015; Chen, Liu and Dai, 2022b).

The previously mentioned isotherms are, however, theoretical, whereas the Freundlich isotherm is an empirical adsorption model that describes reversable adsorption of a non-ideal gas. It also accounts for surface heterogeneity and assumes adsorption enthalpy to exponentially decrease as the surface coverage rises. Freundlich isotherms can be applied to describe multilayer adsorption as well as heterogeneous bond strengths. The latter stems from potential differences in physicochemical properties of the active sites and/or from the surface coverage. Within that, however, as the amount of the "captured" molecules increases, the probability of further multilayer adsorption decreases (suggesting different site monolayer adsorption to be energetically favourable as opposed to multilayer on an "occupied" site). For the above reasons (namely, accounting for non-uniform active site (e.g. a variety of pore sizes and/or shapes) distribution across the surface), this model is often applied to carbonaceous adsorbents, and is described as:

$$q_e = K_F \times P^{1/n} \qquad \textit{Eq. 7}$$

where, q_e is the equilibrium adsorption capacity, mg/g; K_F is the Freundlich constant, mg/(g $bar^{1/n}$); n is the heterogeneity factor, dimensionless; and P is the partial pressure of the gas, bar.

Within this, there are a couple of noteworthy mentions. Firstly, the Freundlich model does not estimate adsorbent's maximum capacity, thus limiting the quality of fitting at higher pressures (Adelodun *et al.*, 2017a). Secondly, an increase of the Freundlich constant is

associated with a simultaneous increase in adsorption capacity of an adsorbent for a given adsorbate. Further, the heterogeneity factor, n, indicates the type of the adsorption process (n < 1 suggests chemisorption, whereas n over 1 is ascribed to physisorption). Lastly, 1/n is often described as the Freundlich intensity parameter, which depicts the magnitude of the adsorption driving force/surface heterogeneity; with 1/n < 1 suggesting favourable adsorption. However, this equation sometimes faces criticism (from the standpoint of fundamental thermodynamics) as at low adsorbate partial pressures the Freundlich model does not reduce to Henry's law (Ho, Porter and McKay, 2002).

Adelodun et al. (Adelodun *et al.*, 2017b) have fitted the Freundlich isotherm to their raw, aminated and potassium-doped carbonaceous adsorbents for carbon capture. This model fit their experimental data well; however, other isotherms were found to be superior, which could be attributed to the lack of a theoretical maximum uptake. Ammendola et al (Ammendola, Raganati and Chirone, 2017), on the other hand, found their CO_2 - AC system to be best described by the Freundlich isotherm.

Toth isotherm model is often used to describe gas-phase adsorption on heterogenous surfaces (and/or multilayer adsorption) due to its applicability at both high and low ends of adsorbate partial pressure range (Terzyk *et al.*, 2003; Ayawei, Ebelegi and Wankasi, 2017; Benzaoui, Selatnia and Djabali, 2018), thus, overcoming a limitation of the Freundlich model. This isotherm is also considered suitable for describing sub-monolayer coverage (Mozaffari Majd *et al.*, 2022), and is expressed as:

$$q_e = \frac{q_{max} \times K_T \times P}{\left(1 + (K_T \times P)^n\right)^{1/n}} \qquad \textit{Eq. 8}$$

where, q_e is the equilibrium adsorption capacity, mg/g; q_{max} – the maximum adsorption capacity, mg/g; K_T is the Toth constant (sometimes referred to as the adsorption affinity), 1/bar; P is the adsorbate pressure, bar; and n is the heterogeneity factor. The latter normally does not equal to 1 (thus, the system is heterogeneous (Ayawei, Ebelegi and Wankasi, 2017)); however, in cases where n=1, the Toth isotherm transform back into its predecessor – the Langmuir isotherm model (i.e. the heterogeneity factor would not impact the isotherm, thus suggesting homogenous adsorbent surface, which is one of the fundamental assumptions of the Langmuir adsorption model). This sorption model has also been extensively applied (and found to fit the experimental data best) within the context of CO_2 adsorption (Serna-Guerrero, Belmabkhout and Sayari, 2010; Schitco *et al.*, 2015; Elfving *et al.*, 2017; Wilson, Gabriel and Tezel, 2020) as well as other adsorbates (Chen, Liu and Dai, 2022b).

In this work, non-linear regression has been employed to fit the experimental data to the models as is suggested in the literature due to the fact that the majority of the described models contain more than two parameters (Kumar *et al.*, 2021). In addition, transforming non-linear equations to a linear form could result in bias (López-Luna *et al.*, 2019). The data has been collected at 25 °C using a stream of pure CO_2. Prior to conducting the experiments, the samples were degassed for 6 hours at 200 °C with a ramping rate of 5 °C/min. The isotherm models with the most accurate fit and the experimental results are presented below in Figure 14, whereas the calculated isotherm parameters, the regression coefficients and the outcome of the error analysis is shown in Table 8.

Table 8. Parameters of the best fit CO_2 adsorption isotherms at 25 °C as well as the results of the error analysis.

Sample	Isotherm Model	Identified parameters	R^2	NRMSE
BA-100-P	Double-site Langmuir	$q_{max\,(1)}$ = 6.011 mg/g $K_{F\,(1)}$ = 7.83 1/bar $q_{max\,(2)}$ = 54.29 mg/g $K_{F\,(2)}$ = 0.2126 1/bar	0.9998	0.01315
AC-Opt	Toth	q_{max} = 286.3 mg/g K_F = 3.423 1/bar n = 0.3171	0.9999	0.00424

Identification of the most well-suited isotherm has been conducted by analysing the results of the error analysis (presented in Table 8) based on the NRMSE and the R^2 values. Interestingly, both of the produced materials have shown to favour either the Dual-site Langmuir or the Toth model (with the virgin carbon favouring slightly more the former and the AC – the latter). This suggests the produced materials to possess a non-uniform pore structure, i.e. surface heterogeneity. The bi-Langmuir model could potentially be explained by the presence of both amorphous and crystalline structures within the virgin carbon, as has been noted in Section 3.2.4.2 (prominent D and G-bands). The activation, on the other hand, has generated a more complex (and, probably non-discrete) heterogeneous surface, potentially leading to a better fit of the Toth isotherm model. This is also in line with the increased number of surface defects on AC-Opt as described in Section 3.2.4.2.

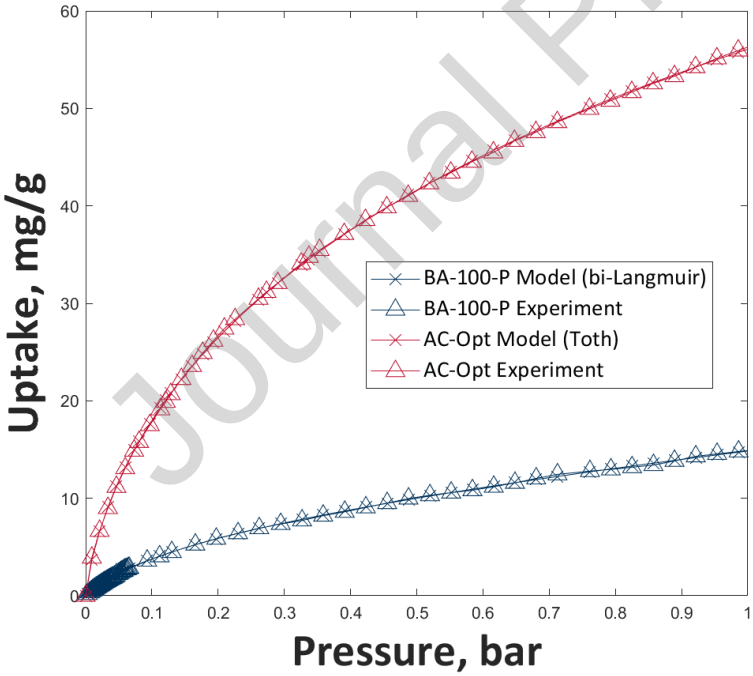

Figure 14. Comparison of experimental data (triangles) and the appropriate equilibrium isotherm models (crosses) for BA-100-P (bottom blue lines) and AC-Opt (top red lines) at 25 °C under pure CO_2.

3.2.6.3. Adsorption Working Capacity

A further aspect of paramount importance is the adsorbent's working capacity. A material that does not get deactivated easily and can withstand changes in temperature (i.e. adsorption/desorption cycles in a temperature swing adsorption process) over a prolonged

period is desired to minimise operational costs. As such, investigations into the working capacity of the adsorbents are an essential step for further technology development.

Figure 15 depicts the cyclic adsorption-desorption steps for the evaluated samples using the fractional coverage (Θ). Θ for every cycle was calculated based on a comparison of the adsorbed amount of CO_2 (on a mg/g basis) to the uptake of the first cycle (i.e. when Θ = 1). Prior to the first adsorption step, the samples were purged under a 50 mL/min flow of N_2 at 150 °C for 30 min and then cooled down (-15°C/min) to 50 °C with the same gas flow rate. Same conditions were used for the desorption steps of the cyclic capacity studies. Upon reaching the desired temperature (i.e. 50 °C), the gas was switched to 50 mL/min of pure CO_2 for the adsorption step.

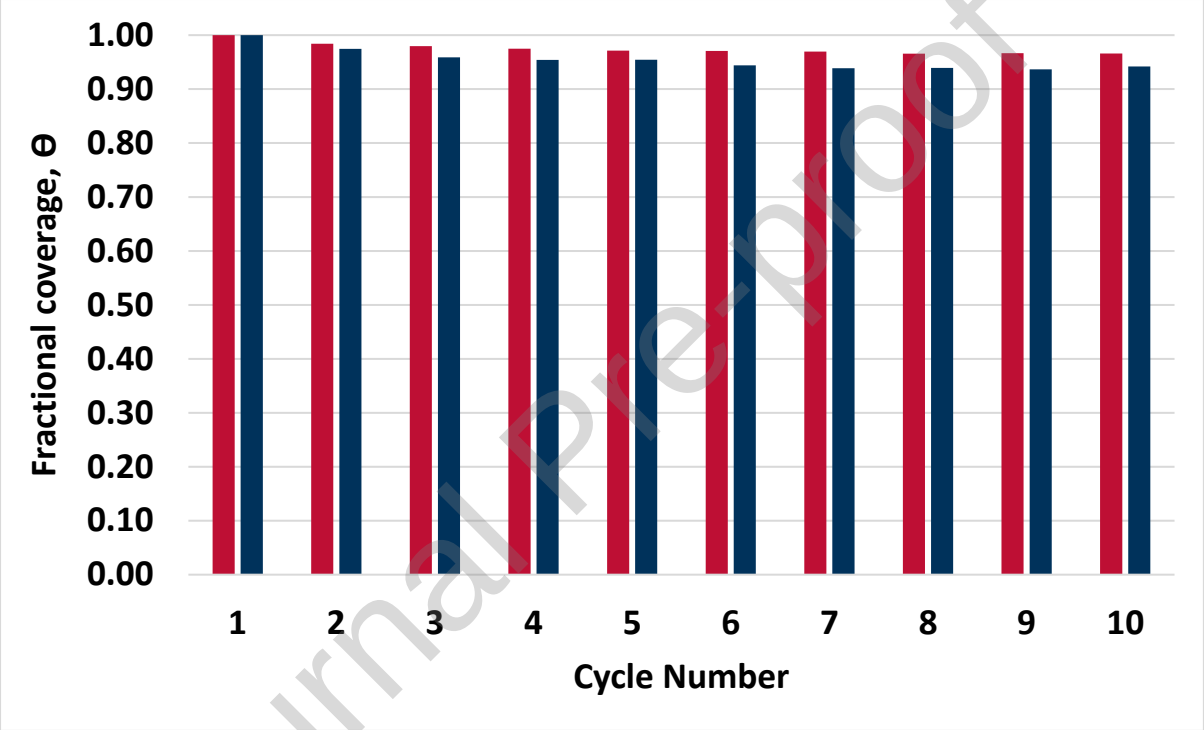

Figure 15. Working capacity of BA-100-P (blue) and AC-Opt (red) over 10 adsorption-desorption cycles.

As can be visualised from Figure 15 the produced sorbents behave similarly. AC-Opt has a minimal loss of uptake over the evaluated range, with the fractional coverage staying above 96%. The virgin BA-100-P also shows good cyclic stability, though, does lose a bigger portion of its adsorption capacity (Θ = 0.94 after 10 cycles). Both evaluated samples present a relatively sharp decrease in mass and uptake from the first cycle to the second one (comparing to later cycle steps), suggesting CO_2 to be more readily desorbed from the surface of the material than moisture/ambient air that were alleviated from the sample during the initial purge. Additionally, high working capacity of the produced sorbents could be ascribed to their high thermal stability, as both materials have been previously exposed to high temperatures (i.e. combustion of the original biomass substance). Further, the slightly stronger cyclic performance of AC-Opt might be associated with the fact that this sample has undergone more extensive thermal treatment (i.e. physical activation) leading to a superior ability to withstand higher temperature regimes.

Further, BA-100-P and AC-Opt cyclic capacities have been evaluated against some alternative sorbents with the results presented in Table 9 below. It should be noted, that in order to draw a fair comparison between different materials, the samples have to undergo adsorption either at the same conditions or following their "ideal" operational envelope. The former, however, would result in some of the materials not reaching equilibrium or not being purged properly and etc, whereas the latter requires prior knowledge of the most beneficial framework for each of the evaluated analogues. These limitations hinder a fair and unbiased comparison between various sorbents.

Table 9. Results of the cyclic adsorption capacity tests.

Sample	CO_2 Uptake, mmol/g	Decrease in Uptake, %	Conditions	Reference
BA-100-P	0.34 (at 50 °C)	6%	Pure CO_2; 10 cycles	This work
AC-Opt	0.69 (at 50 °C)	4%	Pure CO_2; 10 cycles	This work
Commercial AC	0.68 (at 50 °C)	1%	Pure CO_2; 10 cycles	This work
Functionalised carbon nanotube	3.7 (at 25 °C)	6%	Pure CO_2; 10 cycles	(Hao *et al.*, 2020)
Ethylenediamine-modified zeolite type Y	1.4 (at 40 °C)	~21%	15% CO_2; 20 cycles	(Kim *et al.*, 2016)
Polyethyleneimine-impregnated silica	2.8 (at 40 °C)	~74%	15% CO_2; 20 cycles	(Kim *et al.*, 2016)
Tetraethylenepentamine functionalized SBA-15	~2.6 (at 45 °C)	~14%	Pure CO_2; 10 cycles	(Sanz-Pérez *et al.*, 2013)

The drop in uptake for the produced sorbents is somewhat comparable to commercial analogues and lower than the data found in the literature.

However, a paramount aspect of the current research in CCS *via* adsorption lies in the substantial difference in uptake between the "shaped" and the "powder form" adsorbents. This difference is associated with a lesser surface area of the formed particle. However, for fixed bed industrial applications, mm-scale particles are recommended to mimise pressure drop, improve ease of handling and etc. Therefore, this matter of scaling-up from powder to pellet for the biomass combustion bottom ash-derived carbonaceous sorbents is being addressed in our ongoing study. However, echoing the sentiment from Section 1, upon completion of this step, further investigation into the appropriate adsorption regime (e.g. time, flow rate and etc), regeneration mode as well as reactor configuration would be required to "pair" the proposed sorbents with a process that maximises their potential to exploited their full utility.

3.2.7. Economic Evaluation

Apart from the transition from powder to formed shapes, evaluation of the feasibility of the material itself for industrial implementation is of utter importance for transition from

laboratory-scale to large-scale deployment of the technology. However, a comprehensive investigation of the capital and operational expenses is out of the scope of this investigation. Estimation of the manufacturing expenses towards the final product price, however, lacks a well-established procedure (Jaria *et al.*, 2022). By and large, we can conclude that the BA-100-P as well as BA-derived ACs are potentially more economical when compared against the commercially available alternatives due to:

- The absence of a carbonation step, hence lesser energy penalty for carbon production. Electricity consumption is one of the largest contributors towards AC production cost (ranging between approximately 15 – 50 % (Selvaraju and Bakar, 2017a; Wang *et al.*, 2018; Zhang *et al.*, 2019)). Conventional AC production routes deal with a carbon precursor that has to be thermally pre-treated prior to activation. In contrast, BA-100-P (and its derivatives) does not require high temperature carbonisation, hence, further decreasing AC production cost (with the pyrolysis step accounting for 20% (Banerjee *et al.*, 2016), 27% (Mondal *et al.*, 2016) or 39% (Pap *et al.*, 2017) of the total production cost depending on the precursor, thermal treatment conditions and etc.). Moreover, the virgin carbon itself can be used as the capturing media, effectively, negating any energy demand by furnaces/kilns.
- Lack of logistics/transport costs (if deployed *in-situ*), since the BA precursor is available on site. Some estimates of such a cost have been previously shown in the literature to be ~3 % of production cost (Selvaraju and Bakar, 2017b), while others estimated it to be 10% (Pap *et al.*, 2017).
- ACs are often derived from waste-precursors, hence, readily available at little to no cost. Employment of BA-100-P, however, would provide an additional benefit in terms of waste valorisation: decreasing the landfilling costs associated with waste ash. As of 1st April 2022, the standard rate of landfilling tax in the UK is £98.6/tonne, whereas the rate for non-hazardous materials is £3.15/tonne. On top of that, recent government guidance puts considerable emphasis on the importance of biomass waste minimisation, whiles maximising their value as resources ('UK Biomass Policy Statement', 2021).
- Physical activation is less costly (and more eco-friendly) than chemical activation, largely, due to absence of any activating agent in the process, secondary waste generation and additional waste management. For waste plastic ACs, physical activation with CO_2 has been shown to provide viability on an industrial scale as well as the potential for carbon neutrality (Yuan *et al.*, 2022); for oil palm waste, a comparison between physical activation with steam and with CO_2 has suggested a more economical path *via* the latter route (Lai and Ngu, 2021). Additionally, the captured CO_2 could be recycled in the process as the activating gas, further economising the process, and entertaining the principles of circular economy.
- Upon sieving, the top fractions (particle sizes of > 500 μm) nearly exclusively consist of unburnt biomass. These fractions of reclaimed pulverised biomass could be readily reintroduced back into the boiler as fuel, hence increasing the energy intensity of the raw biomass fuel/overall efficiency of the plant. Alternatively, this reclaimed fuel source could be employed in a stand-alone unit providing the required energy for sorbent regeneration, thus significantly reducing the parasitic load inherent to a post-combustion carbon capture process.

- Moreover, reclamation of the top fractions provides another reduction in the quantity of waste ash sent to landfill (in-line with the previously-mentioned government guidance on biomass waste minimisation ('UK Biomass Policy Statement', 2021)), hence a further monetary incentive.

Other less explicit pathways to suppress the cost could be found in:

- Integrating low-grade waste heat (T < 200 °C), a readily on site of a typical thermal power plant, as the heating source for the activation.
- Lowering the T_{act}.
- Increasing the particle size of the virgin carbon (i.e. using a bigger fraction). This would lead to a higher yield during the milling stage, though potentially hampering the purity of the produced carbon.

The commercial AC (CAS 7440-44-0) has a wholesale price of £89.8/kg. Accounting for the comparable CO_2 uptake of AC-Opt, the adsorbent produced in this work may present a more cost-effective approach for adsorbent preparation.

4. Conclusion

Two sorbents were produced using biomass combustion bottom ash. Firstly, the virgin carbon was derived *via* a simple dry extraction technique. This adsorbent has shown a moderate CO_2 uptake; however, due to the miniscule energy requirement for production, this could mean a cost-effective pathway which could help with incentivisation for decarbonisation of the energy sector in the UK. Another driver of reduced cost comes from the minimisation of landfilling expenses for the ash, which also constitutes an additional environmental (i.e. ash management) benefit. The sorbents' performance can be improved using an environmentally-friendly physical activation (low cost and lack of secondary pollution from specific chemical activating agents) for which optimum conditions have been identified. Such activation nearly doubled the CO_2 uptake, making the adsorbent competitive to commercial alternatives for low temperature post-combustion carbon capture. Additionally, both of the produced materials are believed to physically adsorb CO_2.

However, scope for further improvement of the activation process alongside the application aspects also exists. For instance, the matters of evaluation of the CO_2 adsorption capacity of the produced materials under a synthetic flue gas stream. As such, the questions of sorbents' selectivity, behaviour under appropriate post-combustion CO_2 concentrations as well as resistance to moisture (and/or other impurities present in a real flue gas) are yet to be answered. Additionally, in order to overcome financial hurdles associated with carbon capture, a detailed techno-economic analysis (based on a sophisticated accurate process model) of the adsorption unit is also required.

Moreover, since the performance of the optimum sample from activation with CO_2 and N_2 was similar, investigation of the porous structure of the latter material is advisable as this could have a significant positive impact on the commercial production of such activated carbons.

Acknowledgements

This work has been funded by the UK Carbon Capture and Storage Research Centre (EP/W002841/1) through the flexible funded research programme "Investigation of

Environmental and Operational Challenges of Adsorbents Synthesised from Industrial Grade Biomass Combustion Residues". The UKCCSRC is supported by the Engineering and Physical Sciences Research Council (EPSRC), UK, as part of the UKRI Energy Programme.

The authors would like to thank and acknowledge the undergraduate research assistants from the Department of Chemical Engineering at Brunel University London, namely, Anila Islami, Emilie Diaz and Jodie Baker for all their assiatance during this project.

Additionally, we would also like to acknowledge EPSRC Impact Accelerator Award (2022) for their support of this work. Also, the authors would like to recognise the Experimental Techniques Centre (ETC) at Brunel University London and their scientific officers for facilitating access to analytical equipment.

We would like to acknowledge the continued generous support from Drax Group UK, with a special thanks to Dr James Hammerton, Dr Jeni Reeve and Dr Ben Dooley throughout this research.

Bibliography

Adamczuk, A. and Kołodyńska, D. (2015) 'Equilibrium, thermodynamic and kinetic studies on removal of chromium, copper, zinc and arsenic from aqueous solutions onto fly ash coated by chitosan', *Chemical Engineering Journal*, 274, pp. 200–212. doi: 10.1016/j.cej.2015.03.088.

Adelodun, A. A. *et al.* (2017a) 'Isotherm, Thermodynamic and Kinetic Studies of Selective CO2 Adsorption on Chemically Modified Carbon Surfaces', *Aerosol and Air Quality Research*, 16(12), pp. 3312–3329. doi: 10.4209/aaqr.2016.01.0014.

Adelodun, A. A. *et al.* (2017b) 'Isotherm, Thermodynamic and Kinetic Studies of Selective CO2 Adsorption on Chemically Modified Carbon Surfaces', *Aerosol and Air Quality Research*, 16(12), pp. 3312–3329. doi: 10.4209/aaqr.2016.01.0014.

Ammendola, P. *et al.* (2020) 'Fixed bed adsorption as affected by thermodynamics and kinetics: Yellow tuff for CO2 capture', *Powder Technology*, 373, pp. 446–458. doi: 10.1016/j.powtec.2020.06.075.

Ammendola, P., Raganati, F. and Chirone, R. (2017) 'CO2 adsorption on a fine activated carbon in a sound assisted fluidized bed: Thermodynamics and kinetics', *Chemical Engineering Journal*. Elsevier B.V., 322, pp. 302–313. doi: 10.1016/j.cej.2017.04.037.

Antal, M. J. and Grønli, M. (2003) 'The art, science, and technology of charcoal production', *Industrial and Engineering Chemistry Research*, 42(8), pp. 1619–1640. doi: 10.1021/ie0207919.

Assad Munawar, M. *et al.* (2021) 'Biomass ash characterization, fusion analysis and its application in catalytic decomposition of methane', *Fuel*. Elsevier, 285(July 2020), p. 119107. doi: 10.1016/j.fuel.2020.119107.

ASTM (2013) *ASTM D3172-13, Standard Practice for Proximate Analysis of Coal and Coke*. West Conshohocken, PA, USA. Available at: https://www.astm.org/Standards/D3172.htm.

Ayawei, N., Ebelegi, A. N. and Wankasi, D. (2017) 'Modelling and Interpretation of Adsorption Isotherms', *Journal of Chemistry*, 2017. doi: 10.1155/2017/3039817.

Banerjee, S. *et al.* (2016) 'Biosorptive uptake of Fe2+, Cu2+ and As5+ by activated biochar derived from Colocasia esculenta: Isotherm, kinetics, thermodynamics, and cost estimation', *Journal of Advanced Research*. Cairo University, 7(5), pp. 597–610. doi: 10.1016/j.jare.2016.06.002.

Benzaoui, T., Selatnia, A. and Djabali, D. (2018) 'Adsorption of copper (II) ions from aqueous solution using bottom ash of expired drugs incineration', *Adsorption Science & Technology*, 36(1–2), pp. 114–129. doi: 10.1177/0263617416685099.

Brunauer, S., Emmett, P. H. and Teller, E. (1938) 'Adsorption of Gases in Multimolecular Layers', *Journal of the American Chemical Society*, 60(2), pp. 309–319. doi: 10.1021/ja01269a023.

Calzaferri, G., Gallagher, S. H. and Brühwiler, D. (2022) 'Multiple equilibria describe the complete adsorption isotherms of nonporous, microporous, and mesoporous adsorbents', *Microporous and Mesoporous Materials*, 330, p. 111563. doi: 10.1016/j.micromeso.2021.111563.

Chen, R., Liu, J. and Dai, X. (2022a) 'Adsorption equilibrium of ammonia and water on porous adsorbents at low pressure: Machine learning-based models', *Journal of Cleaner Production*, p. 134351. doi: 10.1016/j.jclepro.2022.134351.

Chen, R., Liu, J. and Dai, X. (2022b) 'Adsorption equilibrium of ammonia and water on porous adsorbents at low pressure: Machine learning-based models', *Journal of Cleaner Production*, p. 134351. doi: 10.1016/j.jclepro.2022.134351.

Chindaprasirt, P. and Rattanasak, U. (2019) 'Characterization of porous alkali-activated fly ash composite as a solid absorbent', *International Journal of Greenhouse Gas Control*. Elsevier, 85(April), pp. 30–35. doi: 10.1016/j.ijggc.2019.03.011.

Dai, H. *et al.* (2021) 'A Microwave-Assisted Boudouard Reaction: A Highly Effective Reduction of the Greenhouse Gas CO2 to Useful CO Feedstock with Semi-Coke', *Molecules*, 26(6), p. 1507. doi: 10.3390/molecules26061507.

Derrick, M. R., Stulik, D. and Landry, J. M. (1999) *Infrared Spectroscopy in Conservation Science, Pract Surf Anal by Auger and X-ray Photoelectron Spectrosc*. Los Angeles.

Dhoke, C. *et al.* (2021) 'Review on reactor configurations for adsorption-based CO2 capture', *Industrial and Engineering Chemistry Research*, 60(10), pp. 3779–3798. doi: 10.1021/acs.iecr.0c04547.

Dietrich, F. *et al.* (2018) 'Experimental study of the adsorber performance in a multi-stage fluidized bed system for continuous CO 2 capture by means of temperature swing adsorption', *Fuel Processing Technology*, 173, pp. 103–111. doi: 10.1016/j.fuproc.2018.01.013.

Dixon, T. (2023) *UK Government's Announcement of up to £20bn for CCS, IEA GHG*. Available at: https://ieaghg.org/ccs-resources/blog/uk-government-s-announcement-of-20bn-for-ccs.

EASAC (2018) *Negative emission technologies: What role in meeting Paris Agreement targets?, EASAC Policy Report*. Available at: https://easac.eu/fileadmin/PDF_s/reports_statements/Negative_Carbon/EASAC_Report_on_Negative_Emission_Technologies.pdf.

Elfving, J. *et al.* (2017) 'Modelling of equilibrium working capacity of PSA, TSA and TVSA processes for CO 2 adsorption under direct air capture conditions', *Journal of CO2 Utilization*, 22, pp. 270–277. doi: 10.1016/j.jcou.2017.10.010.

Elliott, W. R. (2022) *Front-End Engineering Design (FEED) Study for a Carbon Capture Plant Retrofit to a Natural Gas-Fired Gas Turbine Combined Cycle Power Plant*. Available at: https://ukccsrc.ac.uk/wp-content/uploads/2022/05/Sherman_FEED_compressed.pdf.

García-Díez, E. *et al.* (2021) 'CO2 capture by novel hierarchical activated ordered micro-mesoporous carbons derived from low value coal tar products', *Microporous and Mesoporous Materials*, 318, p. 110986. doi: 10.1016/j.micromeso.2021.110986.

Gibbins, J. (2022) *The Petra Nova CO2 capture project – why not open it up?, UKCCSRC*. Available at: https://ukccsrc.ac.uk/the-petra-nova-co2-capture-project-why-not-open-it-up/.

Global CCS Institute (2019) *Global Status of CCS, Targeting Climate Change,2019, GCSI*. Available at: https://www.globalccsinstitute.com/wp-content/uploads/2019/12/GCC_GLOBAL_STATUS_REPORT_2019.pdf.

Gómez, M. *et al.* (2020) 'Development of mesoporous materials from biomass ash with future applications as adsorbent materials', *Microporous and Mesoporous Materials*, 299(January). doi: 10.1016/j.micromeso.2020.110085.

Gorbounov, M. *et al.* (2021) 'Application of Nanoporous Carbon, Extracted from Biomass Combustion Ash, in CO2 Adsorption', *Proceedings of the IEEE Conference on Nanotechnology*. IEEE, 2021-July, pp. 229–232. doi: 10.1109/NANO51122.2021.9514288.

Gorbounov, M., Petrovic, B., *et al.* (2022) 'Development of Nanoporosity on a Biomass Combustion Ash-derived Carbon for CO 2 Adsorption', in *2022 IEEE 22nd International Conference on Nanotechnology (NANO)*. IEEE, pp. 245–248. doi: 10.1109/NANO54668.2022.9928660.

Gorbounov, M., Taylor, J., *et al.* (2022) 'To DoE or not to DoE? A Technical Review on & Roadmap for Optimisation of Carbonaceous Adsorbents and Adsorption Processes', *South African Journal of Chemical Engineering*. Elsevier B.V., 41(July), pp. 111–128. doi: 10.1016/j.sajce.2022.06.001.

Guarín Romero, J., Moreno-Piraján, J. and Giraldo Gutierrez, L. (2018) 'Kinetic and Equilibrium Study of the Adsorption of CO2 in Ultramicropores of Resorcinol-Formaldehyde Aerogels Obtained in Acidic and Basic Medium', *C — Journal of Carbon Research*, 4(4), p. 52. doi: 10.3390/c4040052.

Hao, J. *et al.* (2020) 'Hierarchical structure N, O-co-doped porous carbon/carbon nanotube composite derived from coal for supercapacitors and CO 2 capture', *Nanoscale Advances*, 2(2), pp. 878–887. doi: 10.1039/C9NA00761J.

Harvey, O. R. *et al.* (2012) 'Generalized two-dimensional perturbation correlation infrared spectroscopy reveals mechanisms for the development of surface charge and recalcitrance in plant-derived biochars', *Environmental Science and Technology*, 46(19), pp. 10641–10650. doi: 10.1021/es302971d.

Ho, Y. S., Porter, J. F. and McKay, G. (2002) 'Equilibrium isotherm studies for the sorption of divalent metal ions onto peat: Copper, nickel and lead single component systems', *Water, Air, and Soil Pollution*, 141(1–4), pp. 1–33. doi: 10.1023/A:1021304828010.

Hossain, A., Ngo, H. H. and Guo, W. (2013) 'Introductory of Microsoft Excel SOLVER Function - Spreadsheet Method for Isotherm and Kinetics Modelling of Metals Biosorption in Water and Wastewater', *Journal of water sustainability*, 3(4), pp. 223–237. Available at: http://www.jwsponline.com/uploadpic/Magazine/pp223-237 JWS-A-13-013.pdf.

IPCC (2014) *Climate Change 2014, Climate Change 2014: Synthesis Report*. doi: 10.1017/CBO9781107415324.

Jaria, G. *et al.* (2022) 'Overview of relevant economic and environmental aspects of waste-based activated carbons aimed at adsorptive water treatments', *Journal of Cleaner Production*, 344(February), p. 130984. doi: 10.1016/j.jclepro.2022.130984.

Keiluweit, M. *et al.* (2010) 'Dynamic molecular structure of plant biomass-derived black carbon (biochar)', *Environmental Science and Technology*, 44(4), pp. 1247–1253. doi: 10.1021/es9031419.

Ketabchi, M. R. *et al.* (2023) 'Latest advances and challenges in carbon capture using bio-based sorbents: A state-of-the-art review', *Carbon Capture Science & Technology*. Elsevier Ltd, 6(October 2022), p. 100087. doi: 10.1016/j.ccst.2022.100087.

Kiełbasa, K. *et al.* (2021) 'Co2 adsorption on activated carbons prepared from molasses: A comparison of two and three parametric models', *Materials*, 14(23). doi: 10.3390/ma14237458.

Kim, C. *et al.* (2016) 'An ethylenediamine-grafted Y zeolite: a highly regenerable carbon dioxide adsorbent via temperature swing adsorption without urea formation', *Energy & Environmental Science*, 9(5), pp. 1803–1811. doi: 10.1039/C6EE00601A.

Kumar, K. V. *et al.* (2021) 'Probing adsorbent heterogeneity using Toth isotherms', *Journal of Materials Chemistry A*, 9(2), pp. 944–962. doi: 10.1039/D0TA08150G.

Lai, J. Y. and Ngu, L. H. (2021) 'Comparative laboratory cost analysis of various activated carbon activation process', *IOP Conference Series: Materials Science and Engineering*, 1195(1), p. 012018. doi: 10.1088/1757-899x/1195/1/012018.

Li, S. *et al.* (2021) 'A review on biomass-derived CO2 adsorption capture: Adsorbent, adsorber, adsorption, and advice', *Renewable and Sustainable Energy Reviews*. doi: 10.1016/j.rser.2021.111708.

López-Luna, J. *et al.* (2019) 'Linear and nonlinear kinetic and isotherm adsorption models for arsenic removal by manganese ferrite nanoparticles', *SN Applied Sciences*. Springer International Publishing, 1(8), pp. 1–19. doi: 10.1007/s42452-019-0977-3.

Marsh, H. and Rodríguez-Reinoso, F. (2006) 'Activation Processes (Thermal or Physical)', in *Activated Carbon*, pp. 243–321. doi: 10.1016/b978-008044463-5/50019-4.

Masoudi Soltani, S. *et al.* (2015) 'Lead removal from aqueous solution using non-modified and nitric acid-modified charred carbon from the pyrolysis of used cigarette filters', *Desalination and Water Treatment*, 53(1), pp. 126–138. doi: 10.1080/19443994.2013.835751.

Mondal, S. *et al.* (2016) 'Biosorptive uptake of ibuprofen by steam activated biochar derived from mung bean husk: Equilibrium, kinetics, thermodynamics, modeling and eco-toxicological studies', *Journal of Environmental Management*. Elsevier Ltd, 182, pp. 581–594. doi: 10.1016/j.jenvman.2016.08.018.

Mozaffari Majd, M. *et al.* (2022) 'Adsorption isotherm models: A comprehensive and systematic review (2010−2020)', *Science of the Total Environment*. Elsevier B.V., 812(xxxx). doi: 10.1016/j.scitotenv.2021.151334.

Mozgawa, W. *et al.* (2014) 'Investigation of the coal fly ashes using IR spectroscopy', *Spectrochimica Acta - Part A: Molecular and Biomolecular Spectroscopy*. Elsevier B.V., 132, pp. 889–894. doi: 10.1016/j.saa.2014.05.052.

Orenstein, M. and Cooke, B. (2022) 'CCUS in Canada', *Carbon Capture Journal*. Available at: https://www.cer-rec.gc.ca/en/data-analysis/energy-markets/market-snapshots/2019/market-snapshot-carbon-capture-utilization-storage-market-developments.html.

Pap, S. *et al.* (2017) 'Utilization of fruit processing industry waste as green activated carbon for the treatment of heavy metals and chlorophenols contaminated water', *Journal of Cleaner Production*, 162, pp. 958–972. doi: 10.1016/j.jclepro.2017.06.083.

Petrovic, B. *et al.* (2021) 'Biomass Combustion Fly Ash-Derived Nanoporous Zeolites for Post-Combustion Carbon Capture', *Proceedings of the IEEE Conference on Nanotechnology*. IEEE, 2021-July, pp. 233–236. doi: 10.1109/NANO51122.2021.9514342.

Petrovic, B., Gorbounov, M. and Masoudi Soltani, S. (2021) 'Influence of surface modification on selective CO<inf>2</inf> adsorption: A technical review on mechanisms and methods', *Microporous and Mesoporous Materials*, 312. doi: 10.1016/j.micromeso.2020.110751.

Petrovic, B., Gorbounov, M. and Masoudi Soltani, S. (2022) 'Impact of Surface Functional Groups and Their Introduction Methods on the Mechanisms of CO2 Adsorption on Porous Carbonaceous Adsorbents', *Carbon Capture Science & Technology*, 3, p. 100045. doi: 10.1016/j.ccst.2022.100045.

Pham, V. H. *et al.* (2011) 'Chemical functionalization of graphene sheets by solvothermal reduction of a graphene oxide suspension in N-methyl-2-pyrrolidone', *Journal of Materials Chemistry*, 21(10), pp. 3371–3377. doi: 10.1039/c0jm02790a.

Raganati, F., Chirone, R. and Ammendola, P. (2020) 'Calcium-looping for thermochemical energy storage in concentrating solar power applications: Evaluation of the effect of acoustic perturbation on the fluidized bed carbonation', *Chemical Engineering Journal*, 392, p. 123658. doi: 10.1016/j.cej.2019.123658.

Raganati, F., Miccio, F. and Ammendola, P. (2021) 'Adsorption of Carbon Dioxide for Post-combustion Capture: A Review', *Energy & Fuels*, 35(16), pp. 12845–12868. doi: 10.1021/acs.energyfuels.1c01618.

Raizada, P. *et al.* (2017) ' Solar light-facilitated oxytetracycline removal from the aqueous phase utilizing a H 2 O 2 /ZnWO 4 /CaO catalytic system ', *Journal of Taibah University for Science*. Taibah University, 11(5), pp. 689–699. doi: 10.1016/j.jtusci.2016.06.004.

Rashidi, N. A. *et al.* (2012) 'Activated Carbon from the Renewable Agricultural Residues Using Single Step Physical Activation: A Preliminary Analysis', *APCBEE Procedia*, 3, pp. 84–92. doi: 10.1016/j.apcbee.2012.06.051.

Ritchie, H., Roser, M. and Rosado, P. (2020) *CO_2 and Greenhouse Gas Emissions - Our World in Data*, *OurWorldInData.org*.

Rouquerol, J. *et al.* (2013) *Adsorption by Powders and Porous Solids: Principles, Methodology and Applications: Second Edition, Adsorption by Powders and Porous Solids: Principles, Methodology and Applications: Second Edition*. doi: 10.1016/C2010-0-66232-8.

Sajjadi, B., Chen, W. Y. and Egiebor, N. O. (2019) 'A comprehensive review on physical activation of biochar for energy and environmental applications', *Reviews in Chemical Engineering*, 35(6), pp. 735–776. doi: 10.1515/revce-2017-0113.

Sanz-Pérez, E. S. *et al.* (2013) 'CO2 adsorption performance of amino-functionalized SBA-15 under post-combustion conditions', *International Journal of Greenhouse Gas Control*, 17, pp. 366–375. doi: 10.1016/j.ijggc.2013.05.011.

Schitco, C. *et al.* (2015) 'Ultramicroporous silicon nitride ceramics for CO2 capture', *Journal of Materials Research*, 30(19), pp. 2958–2966. doi: 10.1557/jmr.2015.165.

Selvaraju, G. and Bakar, N. K. A. (2017a) 'Production of a new industrially viable green-activated carbon from Artocarpus integer fruit processing waste and evaluation of its chemical, morphological and adsorption properties', *Journal of Cleaner Production*. Elsevier Ltd, 141, pp. 989–999. doi: 10.1016/j.jclepro.2016.09.056.

Selvaraju, G. and Bakar, N. K. A. (2017b) 'Production of a new industrially viable green-activated carbon from Artocarpus integer fruit processing waste and evaluation of its

chemical, morphological and adsorption properties', *Journal of Cleaner Production*. Elsevier Ltd, 141, pp. 989–999. doi: 10.1016/j.jclepro.2016.09.056.

Serna-Guerrero, R., Belmabkhout, Y. and Sayari, A. (2010) 'Modeling CO2 adsorption on amine-functionalized mesoporous silica: 1. A semi-empirical equilibrium model', *Chemical Engineering Journal*, 161(1–2), pp. 173–181. doi: 10.1016/j.cej.2010.04.024.

Sevilla, M. and Fuertes, A. B. (2011) 'Sustainable porous carbons with a superior performance for CO2 capture', *Energy and Environmental Science*, 4(5), pp. 1765–1771. doi: 10.1039/c0ee00784f.

Simonin, J. P. (2016) 'On the comparison of pseudo-first order and pseudo-second order rate laws in the modeling of adsorption kinetics', *Chemical Engineering Journal*. Elsevier B.V., 300, pp. 254–263. doi: 10.1016/j.cej.2016.04.079.

Singh, V. K. and Kumar, E. A. (2016) 'Comparative Studies on CO2 Adsorption Kinetics by Solid Adsorbents', *Energy Procedia*. The Author(s), 90(December 2015), pp. 316–325. doi: 10.1016/j.egypro.2016.11.199.

Sircar, S. (2002) 'Pressure Swing Adsorption', *Industrial & Engineering Chemistry Research*, 41(6), pp. 1389–1392. doi: 10.1021/ie0109758.

Somanathan, T. *et al.* (2015) 'Graphene oxide synthesis from agro waste', *Nanomaterials*, 5(2), pp. 826–834. doi: 10.3390/nano5020826.

Subraveti, S. G. *et al.* (2021) 'Techno-economic assessment of optimised vacuum swing adsorption for post-combustion CO2 capture from steam-methane reformer flue gas', *Separation and Purification Technology*. Elsevier B.V., 256(August 2020), p. 117832. doi: 10.1016/j.seppur.2020.117832.

Sudesh *et al.* (2013) 'Effect of graphene oxide doping on superconducting properties of bulk MgB2', *Superconductor Science and Technology*, 26(9). doi: 10.1088/0953-2048/26/9/095008.

Terzyk, A. P. *et al.* (2003) 'Developing the solution analogue of the Toth adsorption isotherm equation', *Journal of Colloid and Interface Science*, 266(2), pp. 473–476. doi: 10.1016/S0021-9797(03)00569-1.

Thommes, M. *et al.* (2015) 'Physisorption of gases, with special reference to the evaluation of surface area and pore size distribution (IUPAC Technical Report)', *Pure and Applied Chemistry*, 87(9–10), pp. 1051–1069. doi: 10.1515/pac-2014-1117.

Torquato, L. D. M. *et al.* (2017) 'New approach for proximate analysis by thermogravimetry using CO2 atmosphere: Validation and application to different biomasses', *Journal of Thermal Analysis and Calorimetry*, 128(1), pp. 1–14. doi: 10.1007/s10973-016-5882-z.

'UK Biomass Policy Statement' (2021). Department for Business Energy & Industrial Strategy, p. 45. Available at: https://assets.publishing.service.gov.uk/government/uploads/system/uploads/attachment_data/file/1031057/biomass-policy-statement.pdf.

Vijayaraghavan, K. *et al.* (2006) 'Biosorption of nickel(II) ions onto Sargassum wightii: Application of two-parameter and three-parameter isotherm models', *Journal of Hazardous Materials*, 133(1–3), pp. 304–308. doi: 10.1016/j.jhazmat.2005.10.016.

Wang, J. and Guo, X. (2020) 'Adsorption kinetic models: Physical meanings, applications,

and solving methods', *Journal of Hazardous Materials*. Elsevier, 390(November 2019), p. 122156. doi: 10.1016/j.jhazmat.2020.122156.

Wang, Y. *et al.* (2018) 'CO2 adsorption on polyethylenimine-modified ZSM-5 zeolite synthesized from rice husk ash', *Materials Chemistry and Physics*. Elsevier B.V, 207, pp. 105–113. doi: 10.1016/j.matchemphys.2017.12.040.

Wilson, S. M. W., Gabriel, V. A. and Tezel, F. H. (2020) 'Adsorption of components from air on silica aerogels', *Microporous and Mesoporous Materials*, 305, p. 110297. doi: 10.1016/j.micromeso.2020.110297.

Winberg, S. (2020) *Testimony by Steven E. Winberg Assistant Secretary for Fossil Energy U.S. Department of Energy Before the U.S. Senate Committee on Energy and Natural Resources*. Available at: https://www.energy.gov/sites/prod/files/2020/07/f76/7.28.2020 FinalTestimony of Assistant Secretary Steven Winberg CCUS.pdf.

Yaumi, A. L., Bakar, M. Z. A. and Hameed, B. H. (2018) 'Melamine-nitrogenated mesoporous activated carbon derived from rice husk for carbon dioxide adsorption in fixed-bed', *Energy*. Elsevier Ltd, 155, pp. 46–55. doi: 10.1016/j.energy.2018.04.183.

Yuan, X. *et al.* (2022) ' Sustainability-inspired upcycling of waste polyethylene terephthalate plastic into porous carbon for CO 2 capture ', *Green Chemistry*, 24(4), pp. 1494–1504. doi: 10.1039/d1gc03600a.

Zhang, J. *et al.* (2022) 'Carboxylic functionalized mesoporous polymers for fast, highly efficient, selective and reversible adsorption of ammonia', *Chemical Engineering Journal*, 448, p. 137640. doi: 10.1016/j.cej.2022.137640.

Zhang, Y. *et al.* (2019) 'Utilization of wheat bran for producing activated carbon with high specific surface area via NaOH activation using industrial furnace', *Journal of Cleaner Production*. Elsevier Ltd, 210, pp. 366–375. doi: 10.1016/j.jclepro.2018.11.041.

Declaration of interests

☒ The authors declare that they have no known competing financial interests or personal relationships that could have appeared to influence the work reported in this paper.

☐The authors declare the following financial interests/personal relationships which may be considered as potential competing interests:

Highlights

- Waste valorisation could assist *in-situ* decarbonisation of the power sector
- Biomass combustion bottom ash is a promising precursor for carbonaceous adsorbents
- Low temperature physical activation promoted pore declogging
- Two-step optimisation facilitated doubling of adsorption capacity